Article

Synthesis and Characterization of Potent and Safe Ciprofloxacin-Loaded Ag/TiO₂/CS Nanohybrid against Mastitis Causing *E. coli*

Naheed Zafar [1], Bushra Uzair [1,*], Muhammad Bilal Khan Niazi [2], Ghufrana Samin [3], Asma Bano [4], Nazia Jamil [5], Waqar-Un-Nisa [6], Shamaila Sajjad [7] and Farid Menaa [8]

[1] Department of Biological Sciences, International Islamic University, Islamabad 44000, Pakistan; naheedzafar12@gmail.com
[2] School of Chemical and Materials Engineering, National University of Sciences and Technology, Islamabad 44000, Pakistan; bilalniazi2@gmail.com
[3] Department of Chemistry, Faisalabad Campus, University of Engineering and Technology Lahore, Faisalabad 38000, Pakistan; g.samin@uet.edu.pk
[4] Department of Microbiology, University of Haripur, Haripur 22620, Pakistan; asma_baano@yahoo.com
[5] Institute of Microbiology & Molecular Genetics, Punjab University, Lahore 54000, Pakistan; nazia.mmg@pu.edu.pk
[6] Centre for Interdisciplinary Research in Basic and Applied Sciences, International Islamic University, Islamabad 44000, Pakistan; waqarunnisa@iiu.edu.pk
[7] Department of Physics, International Islamic University, Islamabad 44000, Pakistan; shamaila.sajjad@iiu.edu.pk
[8] Department of Nanomedicine and Advanced Technologies, California Innovations Corporation, San Diego, CA 92037, USA; dr.fmenaa@gmail.com
* Correspondence: bushra.uzair@iiu.edu.pk

Abstract: To improve the efficacy of existing classes of antibiotics (ciprofloxacin), allow dose reduction, and minimize related toxicity, this study was executed because new target-oriented livestock antimicrobials are greatly needed to battle infections caused by multidrug-resistant (MDR) strains. The present study aims to green synthesize a biocompatible nanohybrid of ciprofloxacin (CIP)-Ag/TiO₂/chitosan (CS). Silver and titanium nanoparticles were green synthesized using *Moringa concanensis* leaves extract. The incorporation of silver (Ag) nanoparticles onto the surface of titanium oxide nanoparticles (TiO₂NPs) was done by the wet chemical impregnation method, while the encapsulation of chitosan (CS) around Ag/TiO₂ conjugated with ciprofloxacin (CIP) was done by the ionic gelation method. The synthesized nanohybrid (CIP-Ag/TiO₂/CS) was characterized using standard techniques. The antibacterial potential, killing kinetics, cytotoxicity, drug release profile, and minimum inhibitory concentration (MIC) were determined. Field emission scanning electron microscopy (FESEM) and transmission electron microscopy (TEM) revealed spherical agglomerated nanoparticles (NPs) of Ag/TiO₂ with particle sizes of 47–75 nm, and those of the CIP-Ag/TiO₂/CS nanohybrid were in range of 20–80 nm. X-ray diffractometer (XRD) patterns of the hetero system transmitted diffraction peaks of anatase phase of TiO₂ and centered cubic metallic Ag crystals. Fourier Transform Infrared spectroscopy (FTIR) confirmed the Ti-O-Ag linkage in the nanohybrid. The zeta potential of CIP-Ag/TiO₂/CS nanohybrid was found (67.45 ± 1.8 mV), suggesting stable nanodispersion. The MIC of CIP-Ag/TiO₂/CS was 0.0512 µg/mL, which is much lower than the reference value recorded by the global CLSI system (Clinical Laboratory Standards Institute). The CIP-Ag/TiO₂/CS nanohybrid was found to be effective against mastitis causing MDR *E. coli*; killing kinetics showed an excellent reduction of *E. coli* cells at 6 h of treatment. Flow cytometry further confirmed antibacterial potential by computing 67.87% late apoptosis feature at 6 h of treatment; antibiotic release kinetic revealed a sustained release of CIP. FESEM and TEM confirmed the structural damages in MDR *E. coli* (multidrug-resistant *Escherichia coli*). The CIP-Ag/TiO₂/CS nanohybrid was found to be biocompatible, as more than 93.08% of bovine mammary gland epithelial cells remained viable. The results provide the biological backing for the development of nanohybrid antibiotics at a lower MIC value to treat infectious diseases of cattle and improve the efficacy of existing classes of antibiotics by conjugation with nanoparticles.

1. Introduction

The use of antibiotics in the treatment of animal infection and the enhancement of animal health are the main driving forces behind the development of antimicrobial resistance in animal husbandry [1,2]. Drug resistance has been attributed to the over use or misuse of antibiotics in the cattle to treat mastitis, whereas MDR (multidrug-resistant) strains induced mastitis in cattle and are the major cause of economic loss in the dairy industry, and it is also more likely due to irrational use of antibiotics in the dairy industry [3]. In addition, traditional antibiotics have been less effective in the treatment of infectious diseases in dairy cattle. In this context, there is an urgent need for the production of biocompatible antibacterial formulations that could regulate bacterial growth by means of improved and efficient mechanisms [4]. In New York State, a study reported about 82% of milk fed to calves contained residues of antibiotics [5]. Subsequent research studied the effect of the intake of antimicrobial-containing raw milk and identified an increased incidence of antimicrobial resistance in *E. coli* strains of milk/dairy origin [3]. The rise of the antimicrobial resistance is considered a "ticking time bomb" although the WHO (world health organization) has called for a global reduction in veterinary antibiotics to phase out the use of medicinally essential antibiotics by the food industry because of scientific evidence that antimicrobial resistance strains were found in live stocks [6,7]. Ciprofloxacin is a fluoroquinolone class antimicrobial that is widely used for a wide range of infections, including those caused by *E. coli* but resistance is reported against it [8,9].

Nanotechnology is a possible response to antimicrobial resistance, which could promote creativity and create a new generation of antibiotic therapies for potential medicines. Sustaining existing antibiotic activity through novel formulation using nanotechnologies can increase the therapeutic longevity of anti-infection action of existing antibiotics that are no longer effective against MDR strains. There is credible evidence of the effective use of nanotechnologies as antimicrobials [10]. Metal oxide nanoparticles (NPs) as antimicrobial agents demonstrated relatively high efficiency to combat MDR strains. Metal-based nanomaterials, such as silver nanoparticles (AgNPs) and titanium, have attracted immense attention because of their excellent efficiency against MDR bacteria owing to their electronic, optical, and catalytic properties [11]. After the generation of Ag$^+$ and Ti$^+$ ions by the oxidation of Ag NPs, TiO$_2$ eventually induced reactive oxygen radicals (ROS) inside the MDR *E. coli*. The free radicals ($^\bullet$O$_2^-$, $^\bullet$OH, and H$_2$O$_2$) are generated due to the doping of Ag on the surface of TiO$_2$ NPs, which also shifting absorbance of TiO$_2$ NPs from the UV region to visible region of (200–800 nm), enhancing optical properties ultimately and producing ROS species ($^\bullet$O$_2^{--}$, $^\bullet$OH, and H$_2$O$_2$) that cause immediate damage to the MDR *E. coli* and leakage of cellular constituents, leading to the death of the bacterial cell. In addition, it is relatively simple to synthetize AgNPs, and the mass production of metal oxide-based Agnanohybrids is cost-effective [12]. The antimicrobial activity of TiO$_2$ was first reported by Matsunaga and colleagues in 1988. Under near-UV light illumination, microbial cells could be destroyed by contact with a TiO$_2$–Pt [13]. Nanomaterials based on chitosan have gained considerable interest in the biomedical field due to their unusual biodegradability, biocompatibility, and protection against heart diseases, as chitosan could decrease cholesterol absorption and antimicrobial properties [14]. This powerful biopolymer is capable of enhancing the stability of AgNPs and Ag-based nanohybrids [15]. Chitosan-based composite nonmaterials have been reported as highly effective antibacterial agents and found wide applications including in drug delivery, tissue engineering, wound healing, and antibacterial activity [16]. There are many ways to develop new drug delivery systems using liposomes, polymer–drug conjugates, lipid-based nanoparticles, and copolymericcells, which could improve the drug delivery [17].

Recently, the plant-mediated green synthesis of silver nanoparticles has grown into a unique and novel field of nanotechnology. It has gained importance because of its eco-friendly and cost efficiency with lower toxicity as compared to chemical methods [18]. The reduction properties of plant secondary metabolites are responsible for the enhanced ability of plant extracts to produce nanoparticles with enhanced properties [19]. *M. concanensisnimmo* is a medicinal herb with versatile use in pharmaceutical products, antibacterial agent, food source, and water-purifying agent, and it is used for the treatment of variety of diseases including paralysis, menstrual pain, high blood pressure, skin tumors, liver and kidney disease, as well as to treat inflammation of joints, indicating its immense importance in health care industry [20,21].

Considering the urgent need for new clinical interventions to control the global issue of antimicrobial resistance (AMR), a unique ciprofloxacin loaded-TiO_2/Ag/CS nanohybrid was synthesized by the green approach using *M. concanensis* leaves extract. AgNPs and TiO_2NPs were prepared by *M. concanensis* leaves extract, as a reducing and stabilizing agent. The incorporation of AgNPs onto the surface of TiO_2 nanomaterials was performed by the wet chemical impregnation technique. The chitosan (CS) encapsulation of TiO_2/Ag composite followed after coupling with ciprofloxacin (CIP) by the ionic gelation method. Physical characterizations were performed by the routine state-of-the-art techniques of microscopy and spectroscopy. A ciprofloxacin loaded-TiO_2/Ag/CS nanohybrid was tested for its efficacy against MDR strains of *E. coli*-causing mastitis in the cattle by various standard antimicrobial assays indicating the strong antibacterial potential of synthesized nanohybrids. Eventually, we assessed the possible sustained release of the ciprofloxacin from the hybrid material by a drug release kinetics study. Cytotoxicity was evaluated by MTT (3-(4, 5-dimethylthiazol-2-yl)-2, 5-diphenyl tetrazolium bromide) assay for veterinary application using bovine mammary gland cell lines.

2. Experimental Section/Materials & Methods

2.1. Chemicals and Reagents

Ethanol (C_2H_5OH), acetic acid (CH_3COOH), titanium tetraisoproxide (TTP), silver nitrate ($AgNO_3$), and chitosan medium molecular weight (Product number 448877, 75–85% deacetylation, 200–800 cP viscosity of 1% *w/v* in 1% *v/v* acetic acid), pentasodiumtripolyphosphate (TPP), and glacial acetic acid were all purchased from Sigma-Aldrich (Sigma-Aldrich Co., St Louis, MO, USA). Propidium iodide (PI), Annexin V and in the LIVE/DEAD®BacLight™ Bacterial Viability Kit (L7012) (ThermoFisher Scientific, UK), MTT (3-(4, 5-dimethylthiazol-2-yl)-2, 5-diphenyl tetrazolium bromide) assay kit (Cell Proliferation Kit MTT Sigma-Aldrich), Dulbecco's Modified Eagle Medium (DMEM) (Sigma-Aldrich). The Gram staining chemicals, Nutrient Broth (NB), Nutrient Agar (NA), Muller–Hinton Agar (MHA),MacConkey Agar, Brain–Heart Infusion (BHI) broth, andantibiotic discs were all obtained from Oxoid (Thermo Fisher, England, UK), API 20 E system(France, Biomerieux).

2.2. Isolation and Identification of MDR E. coli Strains

MDR *E. coli* strains (N = 87) were isolated from milk samples collected by National Veterinary Laboratories of Pakistan. The California mastitis test was used for the detection of mastitis, and *E. coli* strains were identified using MacConkey agar (Oxoid, UK) as selective medium for selective isolation of *E. coli* from the milk samples. A standard API20E test panel was used for the biochemical-based identification of *E. coli* [22].

2.3. Antibiotic Sensitivity Testing

The disc diffusion assay was used to perform antibiotics sensitivity profiling of isolated *E. coli* strains [22]. According to the antibiotics commonly prescribed for mastitis treatment, the following antibiotic discs were used: Ceftazidime (CAZ) 30 μg, Cefazolin (KZ) 30 μg, Cefoxitin (FOX) 30 μg, Imipenem (IPM) 10 μg, Ceftriaxone (CRO) 30μg, Ampicillin (AMP) 10 μg, Ciprofloxacin (CIP) 5 μg, Meropenem (MEM) 10 μg, Augmentin(AMC) 20 μg,

Gentamicin (CN) 10 μg, Doxycycline (DO) 30 μg, Norfloxacin (NOR) 30 μg, Fosfomycin (FOS) 10 μg, Tetracycline (TE) 30 μg, and Trimethoprim/Sulfamethoxazole (SXT) 30 μg. Discs were placed with the help of a disc dispenser on the MHA (Muller–Hinton Agar) plate and incubated for 24 h at 37 °C. The respective zone of inhibition (ZI) was measured by using a vernier caliper, and the results were compared with those available in the CLSI (Clinical Laboratory Standards Institute) guidelines [23]. A disc dispenser was used to place each disc on pre-inoculated Mueller–Hinton (MH) agar plates, which were incubated for 24 h at 37 °C. Subsequently, ZIs (zones of inhibition) were recorded, and the data were interpreted following CLSI guidelines [24].

2.4. Plant Material Collection and Extract Preparation

M. concanensis was used for the green synthesis of silver and titanium nanoparticles; the collected plant was authenticated by Professor Mushtaq, Department of Botany, QAU Islamabad *M. Concanensis* (Hoon Pakistan). The extract of leaves was used for the synthesis of NPs. The leaves were washed and dried. They were used as a reducing agent for the amalgamation of NPs. A total of 50 g dried leaves was dissolved into 500 mL distilled water (dH_2O) in a beaker and kept on a hot plate at 55 °C for 10 h. The extract has been cooled down at room temperature (RT) and purified for further use.

2.5. Green Synthesis of TiO_2 and Ag Nanoparticles

For the preparation of TiO_2 NPs and AgNPs as shown in Scheme 1, 5 mL of the plant extract was added either to 100 mL titanium tetraisoproxide (TTP) solution (0.4 M) or to 1 mM solution of silver nitrate ($AgNO_3$) under mild magnetic stirring at 28 °C. A change in color of the resultant solution from colorless to brown confirmed the reduction of Ag+ to Ag° moreover in case of TiO_2 color turned to creamy white. Each mixture was centrifuged three times at 12,000 rpm to extract unreacted ions for 10 min. The respective final products were dried at 60 °C, ground, and calcined at 500 °C for 3 h in a muffle furnace to get pure NPs [25].
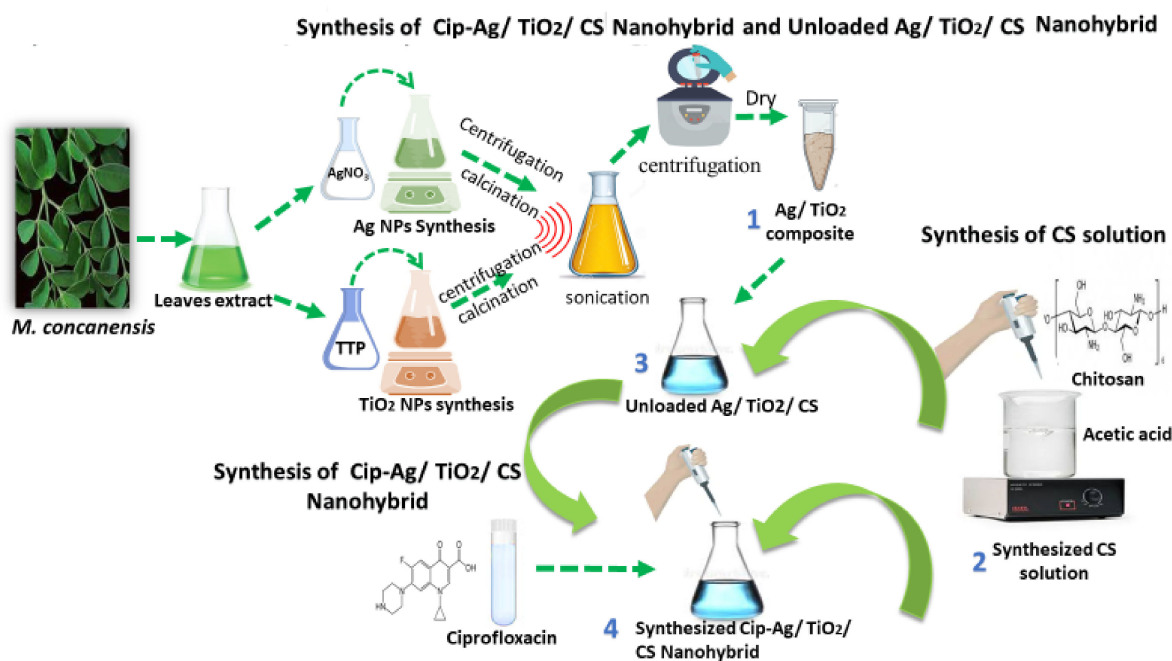
Scheme 1. Green synthesis of nanoformulations using *M. concanensis* leaves extract.

2.6. Formation of TiO_2/Ag Nanocomposite

Ag/TiO_2 nanocomposite was prepared by the wet chemical impregnation method [26]. For that purpose, AgNPs and TiO_2 NPswere mixed in equal amount (0.01 g) into 10 mL

of ethanol, and the mixture was homogenized by sonication for 3 h. The precipitate was obtained after 3–5 times washing and centrifugation at 6000 rpm at 25 °C. The final mixture was dried at 60 °C temperature to obtain the final product Ag/TiO$_2$, as shown in Scheme 1.

2.7. Preparation of CIP-Ag/TiO$_2$/CS Nanohybrid and Unloaded Ag/TiO$_2$/CS

A CIP-Ag/TiO$_2$/CS nanohybrid was obtained by mixing 4 mL of TPP solution containing TiO$_2$/Ag nanocomposite 0.01 g with CIP 0.01 g, and continuous magnetic stirring at 28 °C for 2 h. After complete homogenization of the mixture, the flask was subjected to ultrasonication at 35 Hz for 30 min to scatter the solution particles and agglomeration. Subsequently, the mixture was centrifuged at 14,000 rpm for 30 min at 4 °C [27], the supernatant was discarded, and the pellet was resuspended in ddH$_2$O until use. The same procedure was followed for preparing an unloaded Ag/TiO$_2$/CS nanohybrid; only CIP was eliminated in the reacting mixture, as shown in Scheme 1.

2.8. Physical Characterization of the Green Synthesized Nanoformulations

An X-ray diffractometer (D/MAX 2550, Rigaku Ltd., Tokyo, Japan) was used to determine the crystalline nature and the crystal phase composition of the prepared nanoformulations [28]. The diffraction was observed in the range of 10–80° (2θ) wide-angle XRD using (Cu Kα1 radiation, λ = 1.5406 Å) at 40 kV and 100 mA. The Scherrer equation was used to estimate the crystalline dimension. A Fourier Transform Infrared (FTIR) spectrometer (FT-IR Spectrum 100 spectrometer, PerkinElmer, Waltham, MA, USA)was used to determine the functional groups of unknown elements at 500–5000 cm^{-1} [29]. TEM (JEM 1010, JEOL EU, Nieuw-Vennep, The Netherlands) was used to analyze the size and shape of the nanohybrid at 200 keV, while the selected area electron diffraction (SAED) was used for phase analysis. TEM at 175 nm of scale was also used to study morphological changes in bacterial cells after treatment with CIP-loaded nanohybrid. Field emission scanning electron microscopy (MIRA3TESCAN Inc., Warrendale, PA, USA) photographs at 500 nm scale and EDX (energy-dispersive X-ray) spectra of nanoformulations were used to analyze the size and shape of the nanohybrid. EDX was used to reveal the composition of the elements in the synthesized nanoformulations. The zeta potential of the nanoformulations was measured at room temperature through a Malvern zeta seizer. The electrical charge on the diffused aqueous layer that formed on the surface of the NPs when submerged in water was used to improve the stability of the dosage and the shelf life and to minimize the time and expense of the formulation. The zeta potential and particle size of all the synthesized NPs were measured at room temperature. To perform the following characterizations i.e., XRD, FTIR, TEM, FESEM, and EDX analysis, the dry powder form of all the synthesized nanoformulationswas used directly. To avoid agglomerations of nanoformulations and ensure accuracy, results were obtained after sonication for 40 min. Zeta potential analysis was executed by making suspensions of all the synthesized nanoformulations in the aqueous media.

2.9. Determination of Encapsulation Efficiency

Efficiency of drug encapsulation was determined in accordance with Liu's protocol [30]. A nanophotometer (Implen) was used to measure the quantity of encapsulated CIP into a CIP-TiO$_2$/Ag/CS nanohybrid. The nanohybridwas isolated from the drug-free nanohybrid (i.e., TiO$_2$/Ag/CS) by centrifugation at 10,000 rpm for 25 min, and the supernatant was quantified by spectrophotometry at a wavelength of λ$_{max}$ (295 nm). The encapsulation efficiency (EE) of CIP into CIP-TiO$_2$/Ag/CS nanohybrid was determined using the following equation:

EE = [Loaded CIP into nanohybrid/Total amount of nanohybrid (free + loaded)] × 100

2.10. Antibacterial Activity of Green Synthesized Nanoformulations

The green synthesized nanoformulations, i.e., CIP-Ag/TiO$_2$/CS nanohybrid, unloaded Ag/TiO$_2$/CS nanohybrid, CIP, AgNPs, TiO$_2$NPs, Ag/TiO$_2$ nanocomposite, and

CS were evaluated by the disc diffusion method [24]. The petri plates that contained Muller–Hinton Agar standard media were seeded with MDR strains of *E. coli*. Various concentrations of nanoformulation were screened for anti *E. coli* activity. Sterile filter paper disks were loaded with nanoformulations and placed aseptically on the seeded MH agar plate gently, DMSO was considered as negative control, and unloaded Ag/TiO$_2$/CS nanohybrid discs served as (internal control). The zones of inhibition (ZIs) were recorded after 24 h incubation at 37 °C, the experiment was repeated in triplicate, and SD (standard deviation) was calculated.

2.11. MIC Determination of CIP-Ag/TiO$_2$/CS Nanohybrid

The minimum inhibitory concentration (MIC) of the synthetic antibiotic CIP was determined by using broth microdilution in Nutrient Broth (NB), according to the E-strip method [31]. Briefly, MDR *E. coli* strains suspensions were prepared by comparing the turbidity of the overnight inoculated culture with the 0.5 McFarland standards. Then, each suspension showing turbidity was swabbed with the help of a sterile cotton swab on an MH agar plate, and an E-strip was placed aseptically on the surface of agar. The plates were incubated aerobically for 24 h at 37 °C, after which the data were recorded and analyzed by using a global CLSI-based system [32]. The MIC of the CIP-Ag/TiO$_2$/CS nanohybrid was performed following the broth microdilution method in NB, with a few modifications. Briefly, MDR *E. coli* suspensions showing turbidity according to the 0.5 McFarland standard were added in the test tubes containing different concentrations (0–10 μg/mL) of the CIP-Ag/TiO$_2$/CS nanohybrid before incubation for 18 h at 37 °C. Subsequently, the dilution containing the lowest concentration capable of inhibiting the bacterial growth by displaying visible broth media is called the MIC value. Positive (inoculated broth only) and negative controls (NB only) were included in the experiment.

2.12. Kinetics of Antibacterial Effects of CIP-Ag/TiO$_2$/CS Nanohybrid

In the preliminary experiments, the MIC for each nanoformulation was determined, and exponentially growing *E. coli* cells were used to inoculate a series of tubes containing 2 mL of nutrient broth (Oxoid) (A600 nm 0.05) and a set concentrations of nanoformulations (CIP-Ag/TiO$_2$/CS nanohybrid, unloaded Ag/TiO$_2$/CS nanohybrid, CIP, Ag NPs, TiO$_2$ NPs, Ag/TiO$_2$ nanocomposite, and CS NPs). The time-kill experiments were performed in triplicate and as described by Uzair [33]. Glass flasks that had 50 mL of fresh nutrient broth were inoculated with exponentially growing cells of *E. coli* (A600 nm). Inoculation was carried out following the addition of nanoformulation at the respective concentration of the MIC. The flasks were incubated for 24 h at 30 °C, and the OD (optical density) was calculated at different time points (i.e., 0, 2, 4, 6, 8, 12, and 24 h). The experiment was run in triplicate to authenticate results.

2.13. FESEM Analysis of CIP-Ag/TiO$_2$/CS Nanohybrid

The morphological effect on *E. coli* cells after interaction with CIP-Ag/TiO$_2$/CS nanohybrid at respective MIC concentration was investigated at various time of intervals (i.e., 0, 6, and 12 h) by FE-SEM (Field Emission Scanning Electron Microscopy). Concisely, a tiny drop (10 L) of treated and untreated (control) MDR *E. coli* cells (1×10^4) were put on a glass slide, and slides were placed in 2% glutaraldehyde (GA) and paraformaldehyde HEPES (4-(2-hydroxyethyl)-1-piperazineethanesulfonic acid) buffer (30 mM) for one hour at 37 °C. Then, an increasing concentration of alcohol in water was used for dehydration of the cells, and the slides were kept on water–alcohol solutions for 10 min each in each container having alcohol/water gradient solution. Eventually, slides were washed using ter butyl alcohol for one min, and dried slides were subjected to gold sputter coating for 60 s from three directions before their observation under the FE-SEM microscope (at 2 μm of scale).

2.14. TEM Analysis of CIP-Ag/TiO$_2$/CS Nanohybrid

Ultrastructure changes on *E. coli* log phase cells (1×10^4) were observed under TEM before (control) and after treatment with CIP-Ag/TiO$_2$/CS nanohybrid at respective MIC concentrations for 0, 6, and 12 h. Briefly, 10 μL of treated or untreated bacterial cells were put on a glass slide, which was then fixed using GA 2.5% at 4 °C. After an overnight incubation in GA, the slides were washed with phosphate buffer solution (PBS) 1X. *E. coli* cells were eventually examined under TEM (at 300 nm of field zooming edge)

2.15. Live/Dead Assessment of CIP-Ag/TiO$_2$/CS Nanohybrid-Treated Bacteria

To study Live/Dead *E. coli*, cells treated and untreated with CIP-Ag/TiO$_2$/CS nanohybrid were determined by flow cytometer [34], using AnnexinV and Propidium Iodide (PI) double staining according to the manufacturer's protocol (CUS Ever bright Inc., Suzhou, China). Briefly, a Log-Phase bacterial suspension (1×10^8 CFU/mL) was centrifuged at 3000 rpm for 20 min, and the pellet was resuspended in 50 μL PBS 1X (pH 7.4). Then, *E. coli* cells were exposed to 0.5 μg/μL of CIP-Ag/TiO$_2$/CS nanohybrid in the NB medium at 37 °C and incubated for 6 h. After treatment, *E. coli* cells were centrifuged at 1000 rpm for 15 min, the supernatant was discarded, and the pellet was resuspended in 500 μL of PBS 1X (pH 7.4). The cells were carefully labeled with 10 μL of Annexin V binding buffer and 5 μL of Annexin V-FITC (Fluorescein isothiocyanate) followed by 5 μL of PI stain and incubated in the dark for 20 min at RT, and the resulting stained cells were diluted with 200 μL PBS 1X (pH 7.4) and 400 μL of Annexin binding buffer. After staining, cells were analyzed with FACS (fluorescence-activated single cell sorting) can flow cytometer (Becman Coulter Cytomics FC500).

2.16. Ex Vivo Drug Release Kinetics of CIP-Ag/TiO$_2$/CS Nanohybrid

A Franz diffusion cell was used for ex vivo drug release kinetics studies of the CIP-Ag/TiO$_2$/CS nanohybrid [35]. The skin of a healthy rabbit was taken and fixed between the compartments of the diffusion cell with the donor compartment. Ciprofloxacin (550 μg/mL) alone as control and the CIP-Ag/TiO$_2$/CS nanohybrid solution (at MIC 0.0512 μg/mL present in 3 mL of PBS of pH 7.4) was placed in the donor compartment. The receiver compartment contained 13 mL of PBS of pH 7.4, and the contents were stirred using a magnetic stirrer. The whole assembly was kept at 37 $\pm$ 0.5 °C to maintain normal temperature for skin. Test samples of the nanohybrids (3 mL) were taken at preset time points up to 24 h and replenished with PBS pH 7.4. Samples were purified through a syringe filter, and the drug content of the samples was measured using a UV/visible spectrophotometer (Shimadzu Pharmspec1700, Shimadzu Inst. Japan) at 278 nm. The total sum of the drug released was determined using the formula below.

$$\text{Percent of drug release } (\%) = \frac{\text{Absorbance of sample (nm)}}{\text{Absorbance of control (nm)}} \times 100$$

2.17. Ex Vivo Cytotoxicity Study

To evaluate the cytotoxicity of TiO$_2$/Ag nanocomposites, CSNPs, pure CIP, Ag/TiO$_2$/CS nanohybrids, and CIP-Ag/TiO$_2$/CS nanohybrids, MTT assay [36] was used on bovine mammary gland epithelial cells (BMGE). The cell lines of BMGE tissues were grown on Dulbecco's modified Eagle medium (DMEM) in 96-well plates and then (1×10^5 cells) distributed into wells before incubation for 24 h in the CO$_2$ incubator thermo stated at 37 °C. The viable BMGE cells (1×10^5) were treated with nanoformulations at increasing concentrations (0.2, 0.1, and 0.02 μg/mL) incubated at 37 °C for 24 h, keeping Celecoxib as PC (Positive control) and PBS as controls of the study. Following incubation, 100 μL of fresh DMEM was thoroughly mixed with 10 μL of MTT solution prepared in PBS 1X to replace the existing DMEM [36]. The 96-well plates were incubated again for 4 h. Eventually, 0.1 mL of DMSO solution was used to dissolve the formazan crystals in the wells, and the OD of the wells containing the MTT formazan, which was used as an internal control and BMGE cells treated with nanoformulations at various concentrations were computed at the

reference wavelengths of 570 nm and 620 nm, respectively. The percentage of viability was observed using the given standard equation:

$$\text{Percent cell viability} = \frac{(\text{Test 570 nm} - 620 \text{ nm})}{(\text{Control 570 nm - 620 nm})} \times 100.$$

2.18. Hemolysis Assay

The method for the hemolysis assay of Ag NPs, TiO$_2$ NPs, Ag/TiO$_2$ nanocomposite, unloaded Ag/TiO$_2$/CSNPs, CIP alone, CS NPs, and CIP-Ag/TiO$_2$/CS nanohybrids with PBS (negative control) and Triton 100x (positive control) as controls was performed according to the literature [37]. From the healthy volunteer, blood (3 m) was taken with the help of a sterile syringe in the vacutainers with proper consent of the person, who was informed briefly that the provided blood samples will be exclusively processed for research purposes only. RBCs (red blood cells 1.5 mL) were incubated at 37 °C after treatment with all the synthesized nanoformulations (50 μL) for 6 h, and then spinning was done at 1500 rpm to separate the RBCs from blood. After that, 100 μL of the supernatant of all samples was transferred to a 96-well plate. The absorbance values of the supernatant were taken at 570 nm by using a micro plate reader. The percentage of hemolysis of RBCs was determined by the following equation:

$$\text{Percent (\%) cell viability} = \frac{(\text{Absorbance of Sample} - \text{Negative control})}{(\text{Absorbance of Positive Control} - \text{Negative control})} \times 100.$$

2.19. Ethical Approval and Informed Consent

Pakistan research council regulations were followed in strict accordance with the recommendations in the Guide for the Care and Use of Laboratory Animals of the National Institute of Health (NIH), Islamabad. Experimental protocols (Reg #22-FBAS/PHDBT/F-14) were approved by Institutional Bioethical Committee of International Islamic University, Islamabad.

2.20. Statistics

Mean (SD) was deliberated from independent triplicated experiments. Prevalence was obtained in cross-tabulations and expressed as percentage (%). All statistical analyses were performed using GraphPad Prism 8.1 (GraphPad Software, San Diego, CA, USA).

3. Results and Discussion

3.1. Isolation, Identification, and MIC Determination

E. coli strains were isolated from milk samples producing lactose fermenting pink colonies on MacConkey agar. *E. coli* produced pink colored, smooth, and round colonies [3], which showed the same morphological character of the colony. Under microscope, *E. coli* showed rods, and retained counterstain safranin pink rods of *E. coli* showed a Gram-negative reaction. All the biochemical results were in accordance with previous literature [38]. The rapid identification test for *E. coli*-generated number from API 20E was 5144552. In the present investigation, the disc diffusion method was employed to determine the resistance spectra against multidrug-resistant *E. coli* and the ATCC (8739) strain of *E. coli* as a control organism. The disc diffusion method is the primary tool to classify the strains as an MDR and ESBL (Extended spectrum beta-lactamase) producing *E. coli* strains [32,39]. The results showed that *E. coli* was found highly resistant to the current range of antibiotics, raising concern to find the solution for the emerging resistant Gram-negative rods of mastitis-suffered cattle, as shown in the Figure 1. The minimum inhibitory concentrations were determined by employing the E-strip method and broth microdilution method. Ciprofloxacin by the E-strip method showed more than a 4 μg/mL MIC value by comparing the reference of the global CLSI-based system that is far beyond the recommended dose for *E. coli* [32,39]. Broth microdilution disclosed the MIC of CIP-Ag/TiO$_2$/CS nanohybrid as 0.0512 μg/mL against MDR *E. coli*, which proposed it as an efficient alternative therapeutic agent.
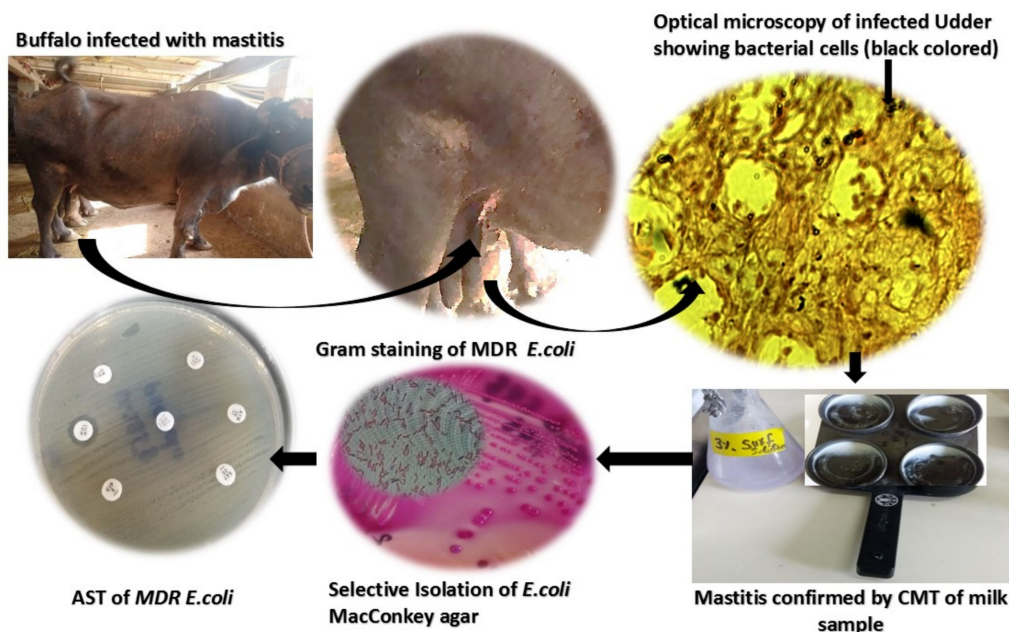
Figure 1. Isolation of multidrug-resistant (MDR) *E. coli* as causative agent of mastitis-induced udder infections in cattle.

3.2. Physical Characterization of the Green Synthetized Nanoformulations

3.2.1. FESEM and TEM Depicted Spherical Morphology and Confirmed the Nano Size of CIP-TiO$_2$/Ag/CS Hybrid

Texture and morphological analyses of greenly synthesized TiO$_2$NPs, AgNPs, Ag/TiO$_2$ nanocomposites, and CIP-Ag/TiO$_2$/CS nanohybrids were determined by FESEM (Figure 2). The the nanostructures of the TiO$_2$NPs, AgNPs, and Ag/TiO$_2$ nanocomposites showed uniform round spherical morphology [40], as illustrated in FESEM micrographs represented by Figure 2A–C, respectively. The particle size ranges of TiO$_2$NPs, AgNPs, Ag/TiO$_2$ nanocomposite CSNPs, and CIP-Ag/TiO$_2$/CS nanohybrids were 25–55 nm, 22–40 nm, 19–35 nm, and 19–75 nm, respectively. This also tentatively confirms the particle sizes observed from XRD analyses. Agglomerated and spherical AgNPs were well dispersed throughout the surface of TiO$_2$ (Figure 2B). It can be remarkably observed from the Ag/TiO$_2$ nanocomposite that AgNPs are incorporated on the surface of TiO$_2$ (Figure 2C). It is noted that there is no distinction between the TiO$_2$NPs and AgNPs in Ag/TiO$_2$ nanocomposites. Eventually, it was clearly seen that the biopolymer CS anchored the whole surface of spherical Ag/TiO$_2$ nanocomposites (Figure 2D). After CS grafting, it was perceived that AgNPs remained segregated onto the TiO$_2$ surface (Figure 2D).

Meanwhile, EDX analysis was done to investigate the elemental distribution of the four nanostructures (Figure 2). Figure 2A displayed the Ti and O signals supporting the TiO$_2$ NP synthesis. Figure 2C revealed the peaks corresponding to the Ti, O, and Ag in Ag/TiO$_2$nanocomposites. It was clear from the signal that a 1.2 wt% nominal content of Ag was closed to its stoichiometric value of 2.0 wt% solution of AgNPs exploited for the fabrication of Ag/TiO$_2$ nanocomposites. The signal of C in Ag/TiO$_2$nanocomposites can be ascribed to the carbon substrate/grid. No additional peaks were observed, which indicated the purity level of the synthesized nanoformulations. Figure 2B showed an elemental profile of AgNPs, which determined the sharp signal of the Ag element. Finally, a synthesized CIP-Ag/TiO$_2$/CS nanohybrid elemental spectrum is shown in Figure 2D, which displayed the peak signals corresponding to TiO$_2$, Ag, TiO$_2$/Ag, and CS, while other peaks or modifications in signal intensity may be attributed to the incorporation of CIP.
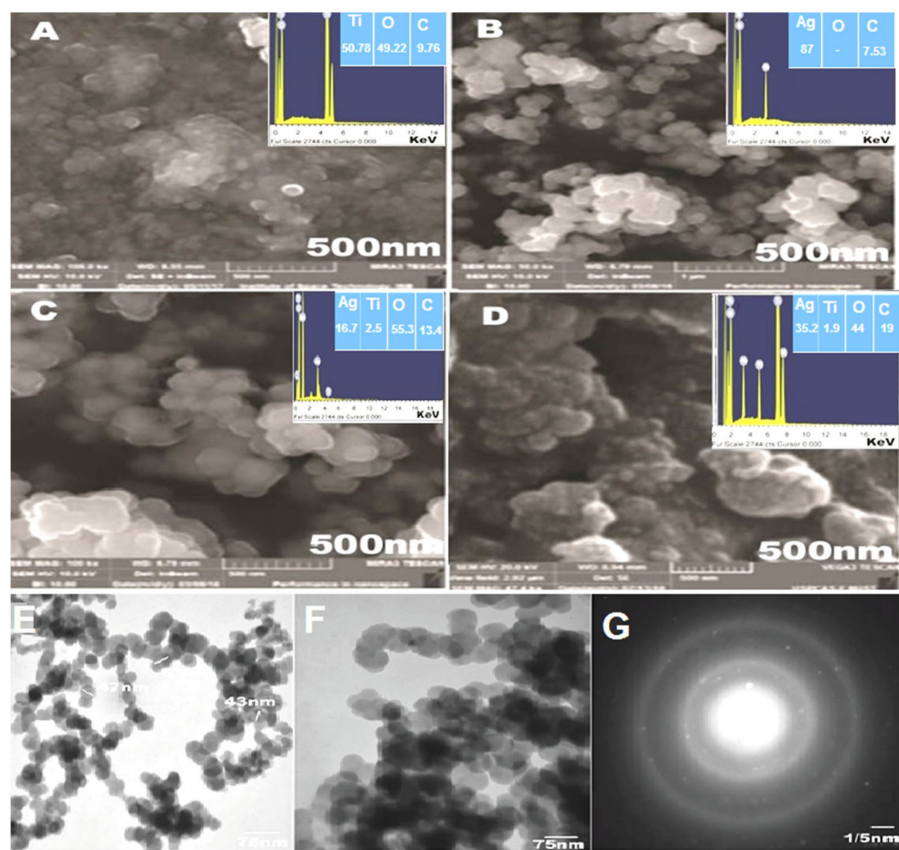
Figure 2. FESEM images of (**A**) TiO$_2$NPs, (**B**) AgNPs, (**C**) TiO$_2$/Ag nanocomposite, (**D**) CIP-TiO$_2$/Ag/CS nanohybrid TEM analysis, (**E**) TiO$_2$/Ag composites, (**F**) CIP-TiO$_2$/Ag/CS nanohybrids, and (**G**) selected area electron diffraction (SAED).

The TEM results confirmed the outcomes of FESEM analysis, as shown in Figure 2E,F, round and spherical morphology was depicted, while the purity of the newly developed CIP-TiO$_2$/Ag/CS nanohybrid was observed by SAED, as shown in Figure 2G. The particle sizes of the Ag/TiO$_2$ composite and CIP-TiO$_2$/Ag/CS nanohybrid were 47–75 nm and 20–80 nm, respectively [28]. The SAED pattern of the prepared CIP-Ag/TiO$_2$/CS nanohybrid demonstrated that Ag/TiO$_2$ contained a face-centered cubic crystalline phase. The SAED pattern further exhibited discrete circular diffraction rings corresponding to the anatase phase of TiO$_2$ NPs. Moreover, SAED showed less agglomeration, which supported the facts that phytocompounds of leaf extract of *M. concanensis* and chitosan contribute their role as previously explained in the literature by Senthilkumar et al., 2019 [41]. Obtained polycrystalline diffraction rings of fabricated spherical NPs were in agreement with previous studies reported by Senthilkumar et al., 2019, Hussein et al., 2021, and Mohamed et al., 2020 [41–43].

3.2.2. XRD, FTIR, and Zeta Potential Analysis of Synthesized Nanoformulations

The XRD pattern of TiO$_2$NPs (Figure 3(Aa)) represented the(101), (004), (200), (105), (211), and (204) plane indices that correspond to the crystalline anatase phase, as supported by (JCPDS No. 84-1285). The XRD peaks of AgNPs (Figure 3(Ab)) show the (111), (200), (220), and (311) crystallographic planes at 2θ° = 38.18°, 44.25°, 64.72°, and 77.40° leading to face-centered cubic metallic silver crystals [44]. It can be inferred that Ag ions (Ag$^+$) are strongly reduced by the *M. concanensis* leaf extract during the synthesis process. Any diffraction peak related to silver oxides was not observed. In the Ag/TiO$_2$ nanocomposite (c in the Figure 3A),the characteristic XRD peaks show the anatase phase of TiO$_2$ and the face-centered cubic silver content without any sign of any other diffraction peaks as

impurity [28]. In CSNPs (d in the Figure 3A), the characteristic XRD peak was indicated at 21.8° crystallinity and the purity of chitosan in the nanostructureis in accordance with Zafar et al., 2020). The XRD profile of the Ag/TiO$_2$/CS nanohybrid (e in the Figure 3A) and the XRD profile of the CIP-Ag/TiO$_2$/CS nanohybrid (f in the Figure 3A) revealed the diffraction peaks of anatase phase of TiO$_2$, Ag and CS NPs. These characteristic peaks were in accordance with previously described peaks of Ag NPs by Lei et al., 2012 [44] while TiO$_2$ and CS peaks correspond to the findings of Zafar et al., 2020 [29]. It is observed that the diffraction peaks of this nanocarrier are shifted to a high angle region, which indicated that foreign material, i.e., CS and CIP, inserted the stress on the lattice of the host material (Ag/TiO$_2$). It is also noted that the leading peak of Ag at 38.18° overlapped with the peak of TiO$_2$ at 38° and suppressed the signal of TiO$_2$.
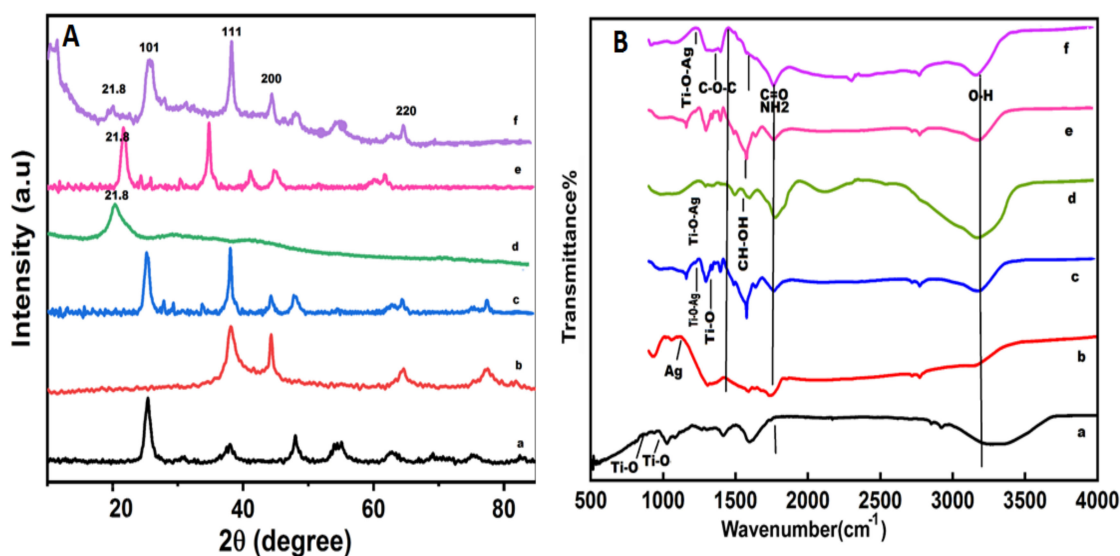

Figure 3. XRD profiles (**A**) and Fourier Transform Infrared spectroscopy (FTIR) spectrums of eco-friendly prepared nanoformulations (**B**) are shown, Key: (**a**) TiO$_2$ NPs, (**b**) AgNPs, (**c**) Ag/TiO$_2$ nanocomposite, (**d**) chitosan (CS) nanoparticles (NPs), (**e**) unloaded Ag/TiO$_2$/CS nanohybrid, and (**f**) CIP-Ag/TiO$_2$/CS nanohybrid.

The crystalline particle size of nanoformulationsis measured about the peaks centered at (101) of anatase TiO$_2$ [45] and (111) of Ag by using Scherrer's equation. The PS (particles size) and the crystalline size of the newly developed drug nanocarrier were 19 nm $\pm$ 1.98 and 0.9821 $\pm$ 0.76 Å respectively. The FTIR spectra of TiO$_2$NPs, AgNPs, CSNPs, Ag/TiO$_2$ nanocomposite, unloaded Ag/TiO$_2$/CS nanohybrids, and CIP-Ag/TiO$_2$/CS nanohybrids are displayed in Figure 3B. The FTIR spectrum of pure TiO$_2$ (Figure 3Ba) exhibited emerging characteristic peaks of absorption at 3408 cm^{-1} that belong to the superposition of the hydroxyl groups (O–H), which evidences the coordination of water molecule to Ti^{4+}cations. The absorption band cantered at 2928 cm^{-1} is assigned to C–H stretching vibrations. The signature at 1603 cm^{-1} can be attributed to C=O stretching vibrations due to the butyl group, organic species as starting precursor solutions, and adsorbed water molecules on the surface of the nanoformulations. The absorption band in the range of 766–610 cm^{-1} is related to the Ti-O bonding that authenticates the formation of TiO$_2$ [46]. The FTIR spectrum of AgNPs (b in the Figure 3B) revealed the characteristic peak at 3424 cm^{-1} corresponding to O−H stretching vibrations of adsorbed water molecules. The peaks at 2919 cm^{-1} and 2841 cm^{-1} indicated alkanes (C–C) stretching vibrations. The signature that appeared at 1625 cm^{-1} is attributed to the bending vibrations of the alkene group [46]. The peak at 1099 cm^{-1} was assigned to the asymmetric and symmetric C=O stretching vibrations due to the carbonyl group present in the leaf extraction. Alkanes, alkenes, and carbonyl groups of leaves extraction are mainly involved in the reduction of Ag$^+$ to AgNPs. The FTIR spectrum of the TiO$_2$/Ag nanocomposite (c in the Figure 3B) displayed band

ranges in the region from 800 to 530 cm^{-1} that are attributed to Ti−O stretching mode and Ti−O−Ag/Ag−O−Tilinkage [40]. The FTIR spectrum of CS (Figure 3Bd) exhibited a high absorption peak of 3423 cm^{-1} and 1636 cm^{-1} due to the availability of a free –OH group from water molecules, an amino group, and a C=O carbonyl moiety group. The value at 1018 cm^{-1} corresponded to the throttle vibration of the C−O−C bond of epoxy or alkoxy. The signatures at 1269 cm^{-1} and 1419 cm^{-1} were due to C−O and CH−OH bonds [46]. The FTIR study of unloaded Ag/TiO$_2$/CS (e in the Figure 3B) characteristic peaks of metal components and CS differential peaks were prominently showed in the spectrum. Moreover, the binary junction of Ti–O and Ag metals was also displayed in the spectrum. The FTIR of CIP-Ag/TiO$_2$/CS nanohybrid (f in the Figure 2B) showed peaks at around 1010 cm^{-1} and 1600 cm^{-1} that are correlated with aromatic bending and stretching. It is clear that the absorption peak centered at 596 cm^{-1} is due to the metal oxygen metal (Ti−O−Ag) mode of vibration.

Zeta potential is the capacity of suspended particles to affect their stability, and the zeta potential greater than 30 mV or less than −30 mV can be distributed permanently in the medium [47]. The zeta potential values of AgNPs (Figure 4a, TiO$_2$NPs (Figure 4b), TiO$_2$/Ag nanocomposite (Figure 4c), and CSNPs (Figure 4d) were −110± 0.5 mV, −123 ± 1 mV, −200 ± 6 mV, and 35.12 ± 2.69 mV, respectively. The newly synthesized CIP-Ag/TiO$_2$/CS nanohybrid showed good stability with a zeta potential value of 67.45 ± 1.8 mV (Figure 4e).

It is worth mentioning that in relation to the adhesion of NPs with bacteria, the surface charge or zeta potential is crucial, since it was demonstrated that positively charged NPs will interact with negatively charged bacteria, and when these bacteria come near positively charged NPs, this ultimately led to the penetration and destruction of bacteria [48,49].
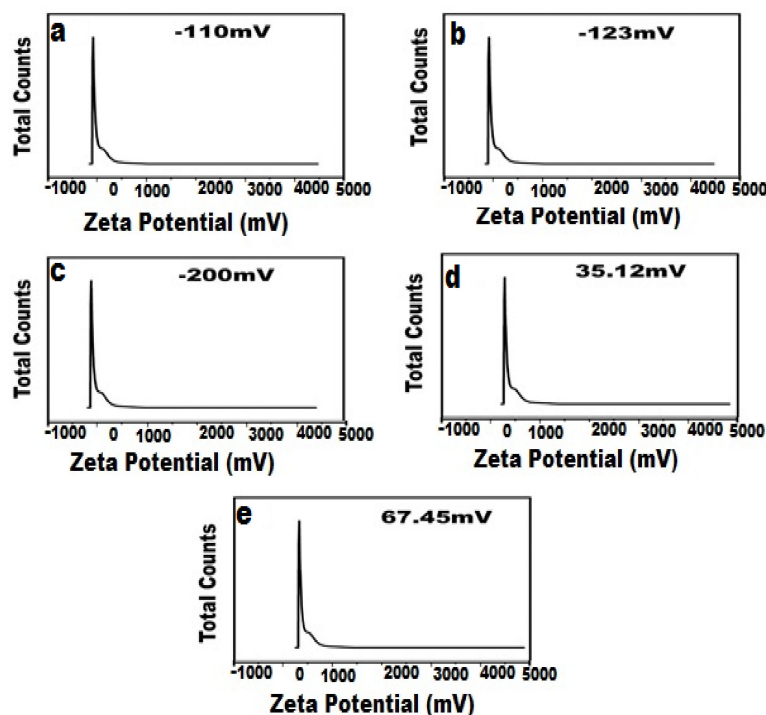
Figure 4. Zeta potential of biosynthesized nanoformulations, (**a**) TiO$_2$NPs, (**b**) AgNPs, (**c**) TiO$_2$/Ag nanocomposite, (**d**) CS, (**e**) CIP-TiO$_2$/Ag/CS nanohybrid.

3.3. Encapsulation Efficiency of CIP-TiO$_2$/Ag/CS Nanohybrid

The encapsulation efficiency of the CIP-TiO$_2$/Ag/CS nanohybrid in the CS system was found as 90% ± 2.07. Hanna and Saadalso reported a good encapsulation efficiency of CIP inside hydrogel made up of chitosan [50].

3.4. Antibacterial Activity of Greenly Synthesized Nanoformulations

Antibacterial activity was studied by the disc diffusion method, as shown in Figure 5. *E. coli* was considered to be MDR on the basis of a resistant pattern against synthetic antibiotics that are generally used for the cure of mastitis, as shown in Figure 5A. Ciprofloxacin was considered the most efficient drug, but according to the present study, it has lost its efficacy; *E. coli* strains have developed resistance against this drug and become super bugs by showing resistance against all the recommended values of MIC, as shown in Figure 5B by employing the E-strip method. The CIP-Ag/TiO$_2$/CS nanohybrid was found to be the most efficient and active antimicrobial agent; the means of zones of inhibition of *E. coli* produced by nanoformulations were measured. Table 1 shows the anti *E. coli* activity of synthesized nanoformulations. As shown in Table 1, the dose-dependent antibacterial property of chitosan, the Ag/TiO$_2$ nanocomposite, and the ciprofloxacin-loaded CS nanohybrid was observed. The CIP-Ag/TiO$_2$/CS nanohybrid exhibited the highest zone of inhibition of 23 mm $\pm$ 1.185 by using 0.2048 µg/mL of the CIP-Ag/TiO$_2$/CS nanohybrid, which is an admirable antibacterial activity.
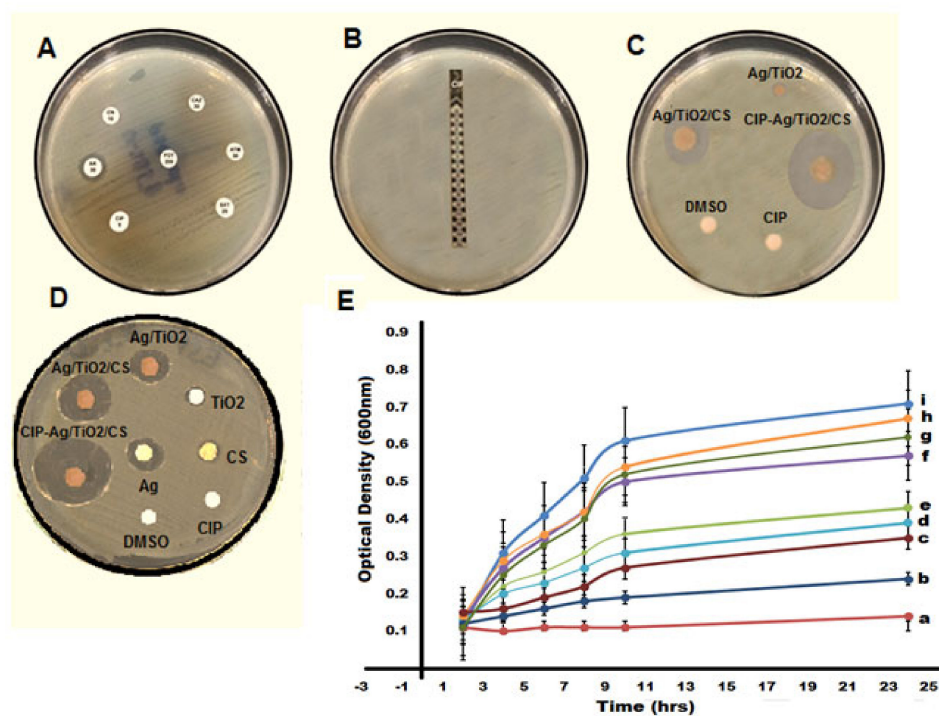
Figure 5. (**A**) Showing resistance pattern of *E. coli* as MDR pathogens, (**B**) displaying the highest minimum inhibitory concentration (MIC) value of ciprofloxacin with no zone by E-strip against *E. coli*, (**C**) zone of inhibition exhibited by synthetic and prepared antimicrobial agents, (**D**) zones of inhibition (ZIs) shown by synthesized nanoformulations at respective MICs, (**E**) kinetics of growth curves for MDR *E. coli* at 0.0512 µg/mL (MIC of nanohybrid), (**a**) NC (Negative control, pure NB), (**b**) CIP-Ag/TiO$_2$/CS nanohybrid, (**c**) unloaded Ag/TiO$_2$/CS, (**d**) Ag/TiO$_2$, (**e**) AgNPs, (**f**) TiO$_2$NPs, (**g**) CS, (**h**) CIP, (**i**) PC (positive control *E. coli* in broth).

Killing Kinetics of Nanoformulations against MDR *E. coli*

According to the current findings, the CIP-Ag/TiO$_2$/CS nanohybrid is highly effective in combating MDR *E. coli*, as reflected in Figure 5E, which presented a growth kinetic curve. The growth of MDR *E. coli* was ceased by the CIP-Ag/TiO$_2$/CS nanohybrid within 6–8 h of incubation by reducing the OD values close to the negative control of the study (autoclaved nutrient broth), as shown in Figure 5E. A study conducted by Li showed an antibacterial attack of Ag NPs, TiO$_2$ NPs, and Ag/TiO$_2$ nanocomposite against MDR *E. coli* [46], but the activity was not as remarkable as observed in this study by our synthesized nanoformulations; particularly, the CIP-Ag/TiO$_2$/CS nanohybrid halted the growth of *E. coli* within a

few hours of exposure. The findings of our analysis showed a mutual antibacterial activity of ciprofloxacin with the Ag/TiO$_2$/CS composite. Shahverdi and colleagues observed improved antibiotic activity against the bacterial panel, using a combination of silver nanoparticles and FDA (Food and Drug Administration) proven antibiotics [51,52].

Table 1. Zone of inhibition and SD (Standard deviation) values of synthesized nanoformulations agents and synthetic antibiotic at various concentrations against MDR *E. coli.*

Antimicrobial Agents	Concentrations (µg/mL) and Zone of Inhibitions (mm)		
	MICs	MICsX2	MICsX3
Loaded CIP-TiO$_2$/Ag/CS	15 ± 1.06	18 ± 0.98	23 ± 1.185
Unloaded TiO$_2$/Ag/CS	7 ± 0.03	9 ± 0.10	10 ± 1.35
Ag/TiO$_2$Nanocomposite	5 ± 0.12	7 ± 0.14	9 ± 1.76
TiO$_2$NPs	2 ± 0.11	9 ± 1.05	11 ± 0.40
Ag NPs	3.5 ± 0.02	8 ± 1.13	12 ± 1.79
CS NPs	1 ± 0.17	3 ± 0.90	7 ± 0.64
CIP	0.9 ± 0.03	2 ± 0.48	5 ± 0.58
DMSO	-	-	-

3.5. MDR E. coli Cell Morphology Alterations Mediated by CIP-TiO$_2$/Ag/CS Nanohybrid

FESEM and TEM have been used to visualize the CIP-TiO$_2$/Ag/CS nanohybrid-induced potential morphological alterations on MDR *E. coli* using respective MIC concentration. After treating the bacterial cells with the CIP-Ag/TiO$_2$/CS nanohybrid, cytolysis in *E. coli* cells can be seen in Figures 6 and 7. In the control group, (untreated) cells shown intact, uniform, and plump morphology as seen in Figures 6A and 7A; however, after 6 h of treatment, the surface of the previously healthy *E. coli* cells showed deep rill-like folds, which led to the detachment of the membrane from the cell wall (Figures 6B and 7B). Almost all cells have low-density regions in their center, which clearly indicates that cytoplasm was damaged by the nanohybrid and the outer membrane was disintegrated, but the cytoplasmic shape was still maintained (Figures 6B and 7B). CIP alone was tested against *E. coli* strains and results were concluded in Figure 6D–F by FESEM and TEM (Figure 7D–F).
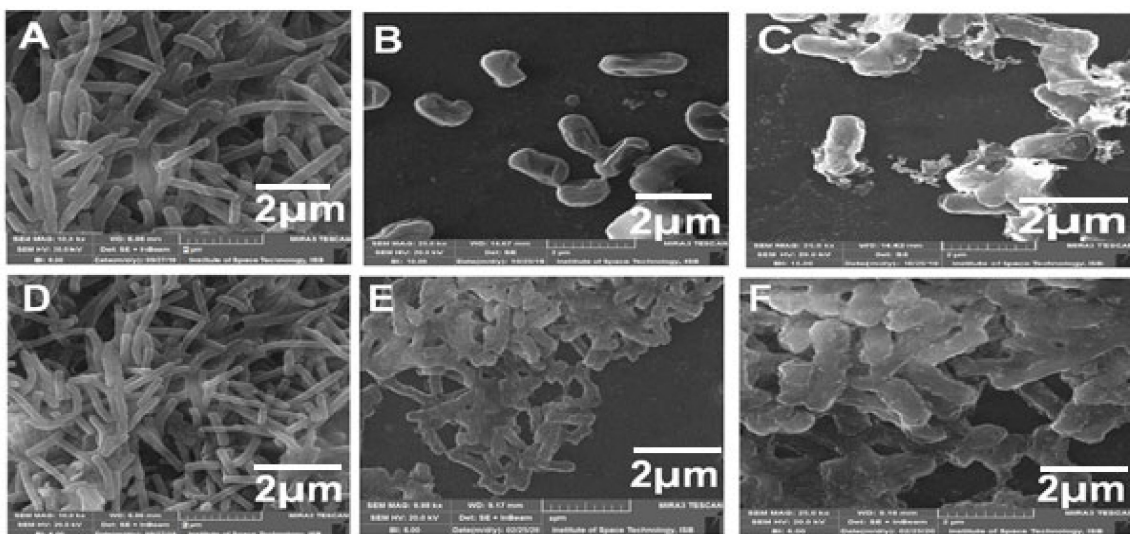
Figure 6. FESEM micrographs displaying morphological changes in MDR *E. coli* cells treated with CIP-Ag/TiO$_2$/CS nanohybridat MIC (0.0512 µg/mL) and at different intervals of time. (**A**) Untreated MDR *E. coli* cells, (**B**) MDR *E. coli* cells after 6 h of incubation, (**C**) MDR *E. coli* cells after 12 h of incubation, (**D**) *E. coli* with CIP at 0 h of incubation, (**E**) CIP at 6 h, and (**F**) CIP at 12 h culture of *E. coli*.
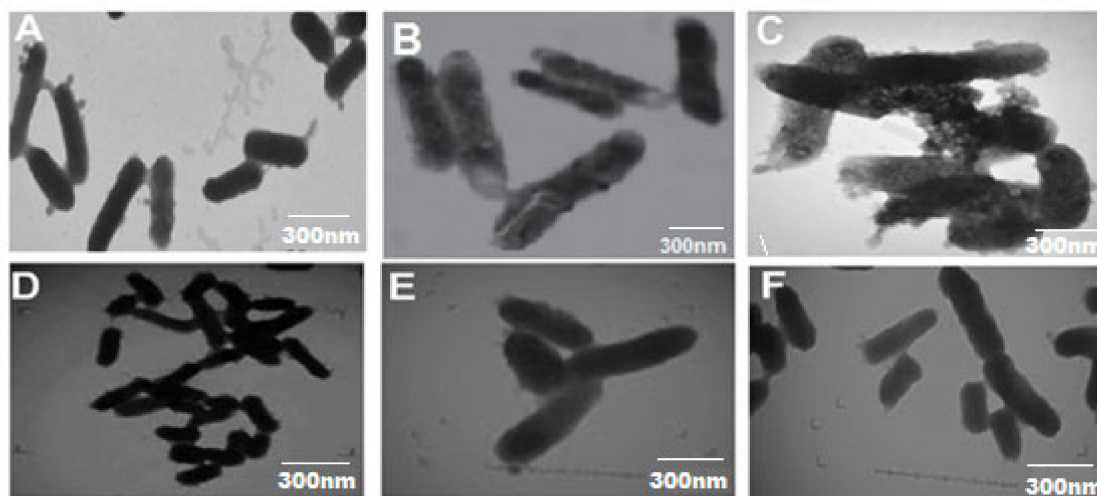
Figure 7. TEM micrographs displaying ultrastructural changes in MDR *E. coli* cells treated with CIP-Ag/TiO$_2$/CS nanohybridat MIC (0.0512 µg/mL) and at different intervals of time. (**A**) Untreated MDR *E. coli* cells, (**B**) MDR *E. coli* cells after 6 h of incubation, (**C**) MDR *E. coli* cells after 12 h of incubation, (**D**) *E. coli* with CIP at 0 h of incubation (**E**) CIP at 6 h, and (**F**) CIP at 12 h of *E. coli* treatment.

### 3.6. Live/Dead Assessment of CIP-Ag/TiO$_2$/CS Nanohybrid-Treated Bacteria

Flow cytometry allows the rapid identification of drug-conjugated nanoparticles internalization in live cells [53]. *E. coli* exhibited increased cell membrane damage and cell inclusion leaking when treated with the CIP-Ag/TiO$_2$/CS nanohybrid, as confirmed by flow cytometry analysis. Annexin V-FITC and PI dyes were used to reveal stages of apoptosis in the *E. coli* cells after interacting with CIP-Ag/TiO$_2$/CS nanohybrid. Phosphatidylserin is a phospholipid abundant in the internal surface of the plasma membrane that is exposed to calcium-dependent signals in the outer leaflet during early apoptosis. PI, an intact impermeable dye can only pass via the cells until it is weakened or dead. In connection with PI, we have obtained a rapid and reliable analysis of cellular structural damage based on a flow cytometric analysis. Our result showed that the cell population in the right upper quadrant in Figure 8B, which indicates late apoptotic cells in comparison to Figure 8A without treatment in which 99.81% cells were live. Current finding semphasizing on the efficacy of nanohybrid by displaying 67.87% of late apoptotic cells and 32.13% cells showed early apoptosis (Figure 8B). Late apoptosis occurred when the nanohybrid penetrated in the *E. coli* cells instigated death, as PI dye is permeable to dead cells only [54]. The *E. coli* cells in the late apoptotic stage were sensitive to Annexin V-FITC dye showing the damaged cell membrane, and the leakage of content was confirmed by PI binding. We have confirmed that cell death caused by CIP-Ag/TiO$_2$/CS nanohybrid displays late apoptotic attributes. Cohesively, data show that the CIP-Ag/TiO$_2$/CS nanohybrid increased the permeation of the *E. coli* cells, potentially leading to cell death.
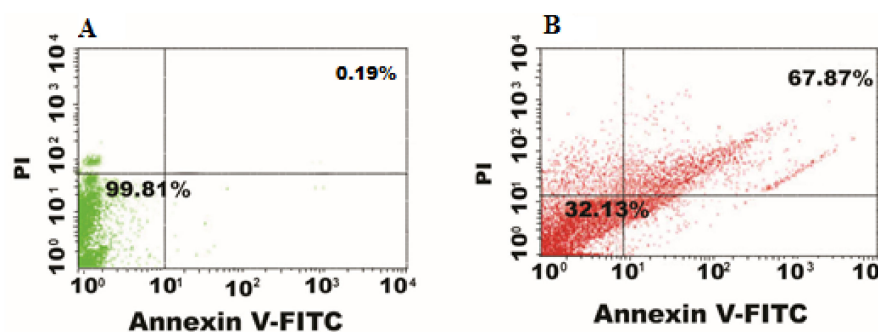
Figure 8. Flow cytometer data nanohybrid-induced cell death. (**A**) control (untreated), (**B**) CIP-TiO$_2$/Ag/CS nanohybrid-treated *E. coli* cells.

3.7. Ex Vivo Drug Release Study CIP-Ag/TiO$_2$/CS Nanohybrid

The exvivo drug release profile of CIP from the CIP-Ag/TiO$_2$/CS nanohybridis presented in Figure 9. The CIP-Ag/TiO$_2$/CS nanohybrid demonstrated the cumulative drug release (89 ± 2.43) at 8hrs of incubation, which was compared to the control value of CIP (94 ± 1.97) during 24 h. Previous study correlates with our findings; slow and sustained release of drug from the cross-linked structure of polymers enclosing antibiotics was reported [55]. The important requirements for designing an efficient delivery system areto ensure the continued and sustained release of the encapsulated drug to the biological system [56]. Our result has confirmed that the drug conjugated with Ag/TiO$_2$/CS nanoparticles and encapsulated in chitosan nanoparticles has improved stability in the acid medium and sustained and prolonged release of the drug. This stability and regulated release is due to chitosan encapsulation and most possibly due to the hydrophilic nature of chitosan. The antibiotic ciprofloxacin was trapped within the polymer matrixof chitosan, which supported the slow release of drugs through the diffusion process. Taken together, our results showed a burst CIF release at 8 h, followed by a sustained release in next 24 h. Shah and co-workers have documented the continued release of moxifloxacin from a nanocomposite of chitosan, and their findings are in agreement with our results [57].
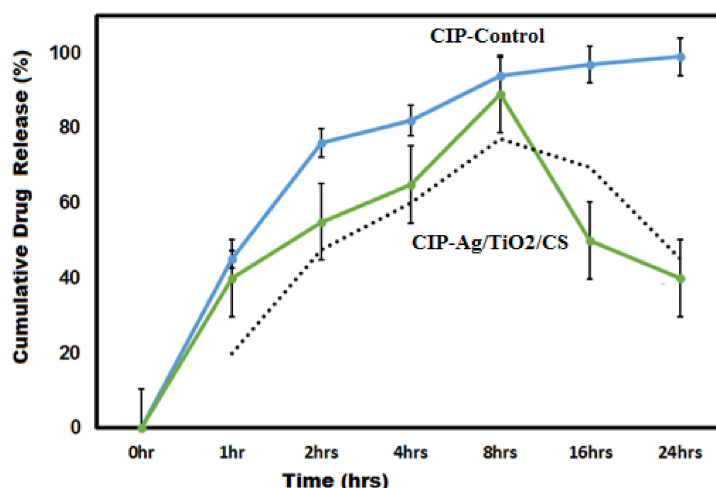

Figure 9. Ex vivo drug release profile of CIP-Ag/TiO$_2$/CS nanohybrid in phosphate buffer solution (PBS, pH 7.4, 37 °C).

3.8. Ex Vivo Cytotoxicity of CIP-Ag/TiO$_2$/CS Nanohybrid on Mammalian Cell Lines and Human RBCs

Since most nanoparticles are semi-synthetic or totally synthetic, in vivo toxicity is critical. Particularly if the nanoparticle contains an antibiotic in a formulation that can affect the normal metabolism of antibiotics, this may reduce the toxicity profile of the antibiotic and allow safer use of these drugs. The potential cytotoxicity at various concentrations (0.02, 0.1, and 0.2 µg/mL) was being analyzed on primary cultures of proliferating bovine mammary gland epithelial cells (BMGE). BMGE cells were found metabolically viable and proliferating after treatment, in a dose-dependent manner with synthesized nanoformulations, which were Ag NPs, TiO$_2$ NPs, TiO$_2$/Ag nanocomposites, CS NPs, pure CIP, Ag/TiO$_2$/CS nanohybrids, and CIP-Ag/TiO$_2$/CS nanohybrids. The cells treated with PBS were used as a negative control, and celecoxib drug was used as positive control. As shown in Figure 10, the viability of BMGE cells was calculated to be 95.23% at lowest concentration (0.02 µg/mL) while 93.08% of cells were viable at the highest concentration of the CIP-Ag/TiO$_2$/CS nanohybrid (0.2 µg/mL). The viability pattern using different concentrations of synthesized nanoformulations are exhibited in Figure 10. Similar results were reported, where chitosan was considered as a safe therapeutic agent due to its nontoxic effect on cell lines [58]. The current study deep-rooted the biocompatibility of

the synthesized nanoformulation for BMGE cells by displaying a good viability pattern. Tomankova reported the cytotoxic effect of Ag NPs in comparison with TiO_2NPs [59], but in our study, chitosan nanoparticles encapsulation masks the cytotoxic effects of these metals.
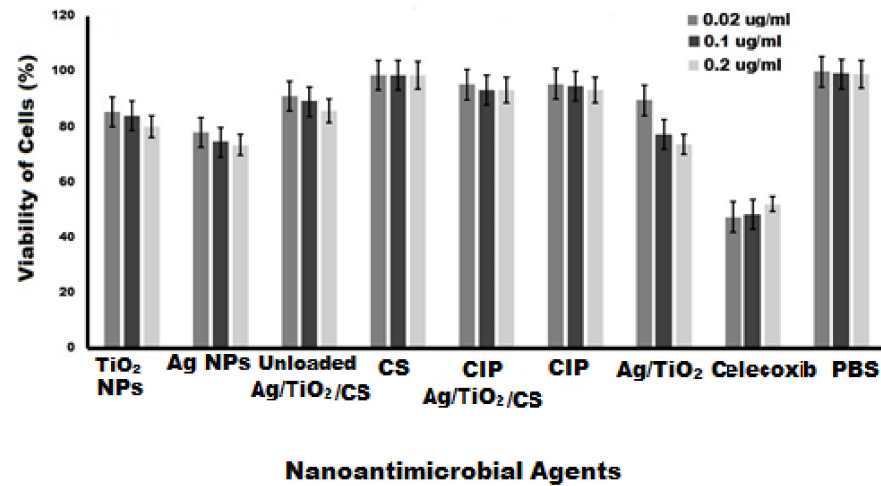
Figure 10. Cytotoxicity analysis of nanoformulations at various concentrations for 24 h of incubation, Celecoxib (PC) and PBS (NC) of study.

The good viability of BMGE cells in the presence of the CIP-Ag/TiO_2/CS nanohybrid is likely due to the indirect exposure of cells to Ag/TiO_2, which is safeguarded by a biocompatible polymer of chitosan nanoparticles, whereas ciprofloxacin is an already approved safe drug.

Blood tissue encounters directly or indirectly with nanoparticles and is able to transport nanoparticles to other cells, tissues, and organs. For this reason, it is highly required to study the toxicity on blood, mainly erythrocytes. In this study, hemolysis assay was designed to study the toxicity on RBCs after exposure to all green synthesized nanoformulations at various concentrations (0.02, 0.1, and 0.2 µg/mL). Nanoformulations allowed interacting for 6 h, and the findings are displayed in Figure 11. Our results revealed that RBCs remained viable after exposure to Ag NPs, TiO_2, Ag/TiO_2, unloaded Ag/TiO_2/CS NPs, pure CIP, and CS NPs; 98.2% viability was observed in CIP-Ag/TiO_2/CS nanohybrid treated red blood cells. The hemotoxicity of TiO_2 NPs was also studied by Li et al., 2008 [60], and the concentration and size-dependent toxicity of Ag NPs was evaluated by Choi et al., 2011 [61]. Hence, newly synthesized CIP-Ag/TiO_2/CS nanohybrids showed negligible hemolysis of RBCS and the proposed hemocompatibility, biocompatibility, and nontoxicity of the CIP-Ag/TiO_2/CS nanohybrid for both human and animal cells.
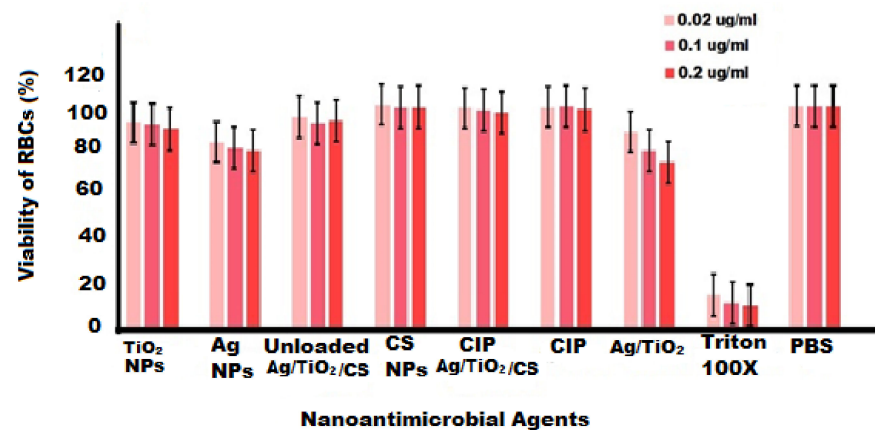
Figure 11. Hemolysis study on human red blood cells (RBCs) with nanoformulations at various concentrations, Triton 100X (PC) and PBS (NC) of study.

3.9. CIP-TiO$_2$/Ag/CS Nanohybrid-Mediated Antibacterial Activity Mechanism

Taken together, our data underline a possible mechanism mediated by the CIP-Ag/TiO$_2$/CS nanohybrid that involved an initial step of adhesion of the particles to the cell wall, which was followed by its destruction of the cell wall (detachment from the outer membrane) to penetrate and disrupt the cell integrity, ultimately leading to apoptotic cell death. Thereby, compared to CIP alone, the enhanced bactericidal effect could be attributed to a synergistic effect of CIP with the TiO$_2$/Ag nanocomposite; moreover, it also showed the surface charges modification of CIP-Ag/TiO$_2$/CS nanohybrid by the biocompatible CS doping. Previous studies [15,62] reported that TiO$_2$/Ba hybrid nanoclusters effectively reduced the cell count for both Gram-positive and Gram-negative bacteria. It was reported that CS can enhance the permeability of the cell membrane via the interaction of anionic groups on the cell [56]. The presence of the –NH bond is important for antimicrobial activity of CS [63]. Then, CIP anchoredto CS triggers the liberation of Ag$^+$ from the nanohybrid material, enhancing Ag$^+$ penetration/entrance into the cell through the cell membrane, and subsequently enhancing the ROS levels, leading to cell death [64]. Meanwhile, it is known that TiO$_2$ further disrupts the barrier properties of the outer membrane of the bacteria by ROS [60,64]. CIP is an exceeding energetic antibiotic against diverse microorganisms and effectively causes double-stranded DNA (dsDNA) breaks and inhibits the DNA gyrase [65]. Eventually, the synergistic action of each entity of the newly biosynthetized nanohybrid has led to the disruption of the cell membrane and ROS-mediated oxidative stress, resulting in enhanced antibacterial activity (Figure 12).
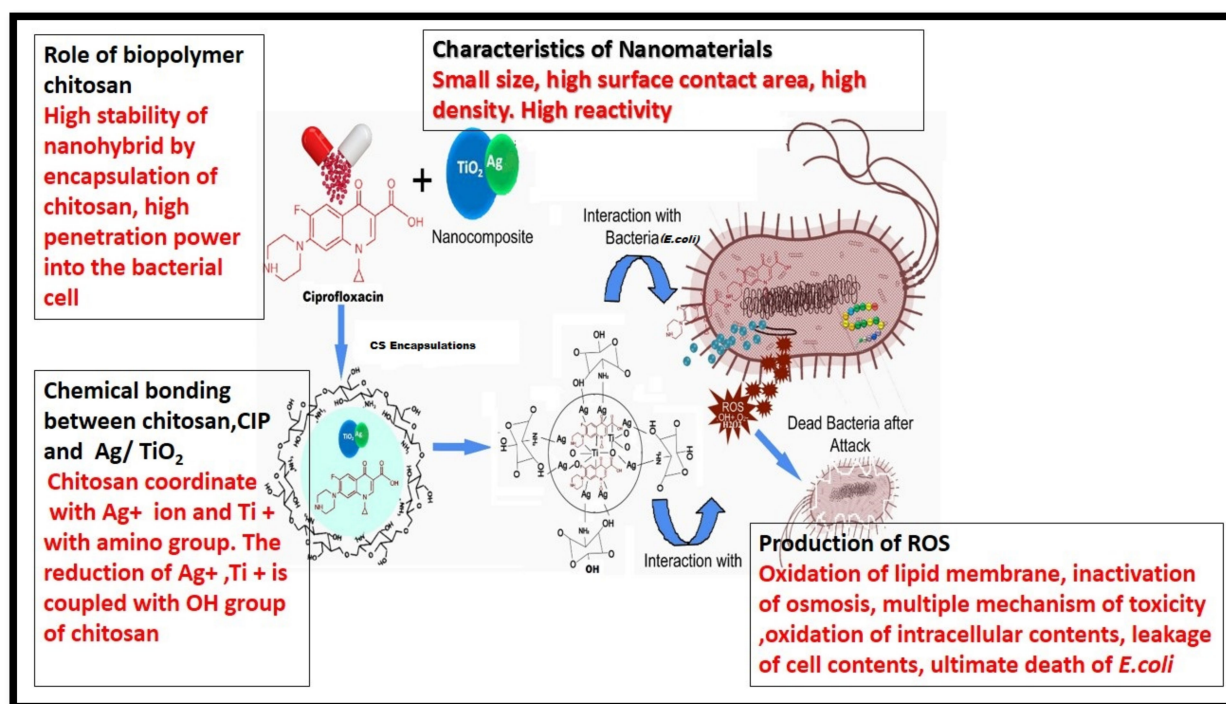

Figure 12. Putative CIP-TiO$_2$/Ag/CS nanohybrid-mediated cellular and molecular bactericidal mechanism.

The newly developed CIP-Ag/TiO$_2$/CS nanohybrid has been prepared by using a unique leaf extract of *Moringa concanensis*, which has been less explored for the synthesis of nanoparticles. This newly developed CIP-Ag/TiO$_2$/CS nanohybrid is not reported to treat mastitis caused by MDR *E. coli.* The nanoparticles obtained in the study had a small particle size (20–40 nm) and suitable polarity (67.45 $\pm$ 1.8 mV) due to chitosan encapsulation, which may increase the drug penetration into the MDR *E. coli* cells, as evident by flow cytometry and improve its antibacterial activity to overcome the resistance mechanism. The results showed that the CIP-Ag/TiO$_2$/CS nanohybrid can successfully

inhibit the growth of MDR *E. coli* strikingly with an MIC value lower than the MIC of ciprofloxacin itself. It was anticipated that the CIP-Ag/TiO$_2$/CS nanohybrid could be applied broadly in the treatment of livestock infectious diseases (mastitis) as an alternative therapeutic agent in the field of medicine due to highly biocompatibilities.

4. Conclusions and Perspectives

This research was conducted to improve the effectiveness of existing groups of antibiotics (ciprofloxacin) and to reduce dosage and mitigate the associated toxicity. This study illustrates the successful development of a CIP-Ag/TiO$_2$/CS nanohybrid. The eco-friendly synthesized CIP-Ag/TiO$_2$/CS nanohybrid exerted excellent antibacterial activity at relatively very low MIC compared to CIP alone. The synthesis of Ag/TiO$_2$ occurred through reduction of *M. concanensis* leaves extract followed by an ionic gelation method for the conjugation of CIP and CS encapsulation. The excellent rapid anti *E. coli* activity was exhibited by our synthesized nanohybrid formulation. Flow cytometry revealed cell membrane damage leading to cell lysis as confirmed by SEM and TEM, as major morphological alterations were seen in *E. coli* cells. The encapsulation efficiency of the CIP-TiO$_2$/Ag/CS nanohybrid in the CS matrix was calculated 90% $\pm$ 2.07. Drug released kinetics exhibited sustained drug release from the nanohybrid. The nanohybrid was proved to be safe and nontoxic on bovine mammary gland epithelial cells. Further in vivo experiments should be performed to investigate the biocompatibility and undesired adverse effects for their possible therapeutic use. The use of available antibiotics conjugated or attached to nanoparticles offers an alternate angle to antibiotic therapy.

Author Contributions: Conceptualization, B.U.; and N.Z.; methodology, M.B.K.N.; software, N.J.; validation, G.S., and W.-U.-N.; formal analysis, F.M., N.J., A.B.; investigation, N.Z. and F.M.; resources, N.J., S.S.; data interpretation, N.Z. and F.M.; writing—original draft preparation, N.Z.; review and editing, B.U. and F.M.; visualization, M.B.K.N.; supervision, B.U.; project administration, M.B.K.N. All authors have read and agreed to the published version of the manuscript.

Institutional Review Board Statement: The present study was approved by Institution Review Board and Ethical Review Board of International Islamic University, Islamabad, Pakistan (Reg #22-FBAS/PHDBT/F-14).

Informed Consent Statement: Consent was obtained from all volunteers involved in the study, informed briefly that the provided blood samples will be exclusively processed for research purpose only.

Data Availability Statement: Article contains all the related data and information.

Conflicts of Interest: The authors declare no conflict of interest.

References

1. Kimera, Z.I.; Mshana, S.E.; Rweyemamu, M.M.; Mboera, L.E.G.; Matee, M.I.N. Antimicrobial use and resistance in food-producing animals and the environment: An African perspective. *Antimicrob. Resist. Infect. Control* **2020**, *37*, 1–12. [CrossRef]
2. Ventola, C.L. The Antibiotic Resistance Crisis: Part 1: Causes and Threats. *Pharm. Ther.* **2015**, *40*, 277–283.
3. Pereira, R.V.V.; Siler, J.D.; Bicalho, R.C.; Warnick, L.D. In vivo selection of resistant *E. coli* after ingestion of milk with added drug residues. *PLoS ONE* **2014**, *9*, e115223. [CrossRef]
4. Abid, S.; Uzair, B.; Niazi, M.B.H.; Fasim, F.; Bano, S.A.; Jamil, N.; Batool, R.; Sajjad, S. Bursting the virulence traits of MDR Strains of *Candida albicans* using sodium alginate based microspheres containing nystatin loaded MgO/CuO nanocomposites. *Int. J. Nanomed.* **2021**, *16*, 1157–1174. [CrossRef]
5. Pereira, V.V.R.; Lima, S.; Siler, J.D.; Foditsch, C.; Warnick, L.D.; Bicalho, R.C. Ingestion of milk containing very low concentration of antimicrobials: Longitudinal effect on fecal microbiota composition in preweaned calves. *PLoS ONE* **2016**, *11*, e0147525.
6. Agga, G.E.; Arthur, T.M.; Durso, L.M.; Harhay, D.M.; Schmidt, J.W. Antimicrobial-resistant bacterial populations and antimicrobial resistance genes obtained from environments impacted by livestock and municipal waste. *PLoS ONE* **2015**, *10*, e0132586. [CrossRef]

7.   World Health Organization. Global Priority List of Antibiotic-Resistant Bacteria to Guide Research, Discovery, and Development of New Antibiotics. 2017. Available online: http://www.who.int/medicines/publications/global-priority-list-antibiotic-resistantbacteria/en/ (accessed on 27 February 2017).

8.   Anderson, V.E.; Gootz, T.D.; Osheroff, N. Topoisomerase IV catalysis and the mechanism of quinolone action. *J. Biol. Chem.* **1998**, *273*, 17879–17885. [CrossRef] [PubMed]

9.   Van der Putten, B.C.L.; Remondini, D.; Pasquini, G.; Janes, V.A.; Matamoros, S.; Schultsz, C. Quantifying the contribution of four resistance mechanisms to ciprofloxacin MIC in *Escherichia coli*: A systematic review. *J. Antimicrob. Chemother.* **2018**, *74*, 298–310. [CrossRef]

10.   Kumar, M.; Curtis, A.; Hoskins, C. Application of Nanoparticle Technologies in the Combat against Anti-Microbial Resistance. *Pharmaceutics* **2018**, *10*, 11. [CrossRef] [PubMed]

11.   Slavin, Y.N.; Asnis, J.; Häfeli, U.O.; Bach, H. Metal nanoparticles: Understanding the mechanisms behind antibacterial activity. *J. Nanobiotechnol.* **2017**, *15*, 1–20. [CrossRef] [PubMed]

12.   Kandi, V.; Kandi, S. Antimicrobial properties of nanomolecules: Potential candidates as antibiotics in the era of multi-drug resistance. *Epidemiol. Health* **2015**, *37*, e2015020. [CrossRef]

13.   Gnanaprakasam, A.; Sivakumar, V.; Sivayogavalli, P.; Thirumarimurugan, M. Characterization of TiO₂ and ZnO nanoparticles and their applications in photocatalytic degradation of azodyes. *Ecotox. Environ. Saf.* **2015**, *121*, 121–125. [CrossRef]

14.   Kravanja, G.; Primožič, M.; Knez, Z.; Leitgeb, M. Chitosan-Based (Nano) Materials for Novel Biomedical Applications. *Molecules* **2019**, *24*, 1960. [CrossRef]

15.   Marta, B.; Potara, M.; Iliut, M.; Jakab, E.; Radu, T.; Imre-Lucaci, F.; Katona, G.; Popescu, O.; Astilean, S. Designing chitosan–silver nanoparticles–graphene oxide nanohybrids with enhanced antibacterial activity against *Staphylococcus aureus*. *Colloids Surf. A Physicochem. Eng. Asp.* **2015**, *487*, 113–120. [CrossRef]

16.   Elgadir, M.A.; Uddin, M.S.; Ferdosh, S.; Adam, A.; Chowdhury, A.J.K.; Sarker, M.Z.I. Impact of chitosan composites and chitosan nanoparticle composites on various drug delivery systems: A review. *J. Food Drug Anal.* **2015**, *23*, 619–629. [CrossRef]

17.   Thu, H.P.; Nam, N.H.; Quang, B.T.; Son, H.A.; Toan, N.L.; Quang, D.T. In vitro and in vivo targeting effect of folate decorated paclitaxel loaded PLA–TPGS nanoparticles. *Saudi Pharm. J.* **2015**, *23*, 683–688. [CrossRef]

18.   Zhang, X.F.; Liu, Z.G.; Shen, W.; Gurunathan, S. Silver nanoparticles: Synthesis, characterization, properties, applications, and therapeutic approaches. *Int. J. Mol. Sci.* **2016**, *17*, 1534. [CrossRef]

19.   Basiuk, V.A.; Basiuk, E.V. *Green Processes for Nanotechnology; From Inorganic to Bioinspiring Nanomaterials*; Springer International Publishing: Cham, Switzerland, 2015; pp. 35–73.

20.   Anbazhakan, S.; Dhandapani, R.; Anandhakumar, P.; Balu, S. Traditional Medicinal Knowledge on *Moringa concanensis* Nimmo of Perambalur District, Tamilnadu. *Anc. Sci. Life* **2007**, *26*, 42–45. [PubMed]

21.   Balamurugan, V.; Balakrishnan, V. Evaluation of phytochemical, pharmacognostical and antimicrobial activity from the bark of *Moringa concanensis* Nimmo. *Int. J. Curr. Microbiol. Appl. Sci.* **2013**, *2*, 117–125.

22.   Unnerstad, H.E.; Lindberg, A.; Waller, K.P.; Ekman, T.; Artursson, K.; Nilsson-Öst, M.; Bengtsson, B. Microbial aetiology of acute clinical mastitis and agent-specific risk factors. *Vet. Microbiol.* **2009**, *137*, 90–97. [CrossRef]

23.   Morrissey, I.; Bouchillon, S.K.; Hackel, M.; Biedenbach, D.J.; Hawser, S.; Hoban, D.; Badal, R.E. Evaluation of the Clinical and Laboratory Standards Institute phenotypic confirmatory test to detect the presence of extended-spectrum β-lactamases from 4005 *Escherichia coli*, *Klebsiellaoxytoca*, *Klebsiella pneumoniae* and *Proteus mirabilis* isolates. *J. Med. Microbiol.* **2014**, *63*, 556–561. [CrossRef] [PubMed]

24.   Barker, K. *At the Bench: A Laboratory Navigator*; Cold Spring Harbor Laboratory Press: Cold Spring Harbor, NY, USA, 1998.

25.   Yadav, M.; Kaur, P. A review on exploring phytosynthesis of silver and gold nanoparticles using genus Brassica. *Int. J. Nanopart.* **2018**, *10*, 165–177. [CrossRef]

26.   Shameli, K.; Ahmad, M.B.; Zargar, M.; Yunus, W.M.; Rustaiyan, A.; Ibrahim, N.A. Synthesis of silver nanoparticles in montmorillonite and their antibacterial behavior. *Int. J. Nanomed.* **2011**, *6*, 581–590. [CrossRef] [PubMed]

27.   Jamil, B.; Habib, H.; Abbasi, S.A.; Ihsan, A.; Nasir, H.; Imran, M. Development of cefotaxime impregnated chitosan as nano-antibiotics: De novo strategy to combat biofilm forming multi-drug resistant pathogens. *Front. Microbiol.* **2016**, *7*, 330. [CrossRef] [PubMed]

28.   Yang, X.H.; Fu, H.T.; Wang, X.C.; Yang, J.L.; Jiang, X.C.; Yu, A.B. Synthesis of silver-titanium dioxide nanocomposites for antimicrobial applications. *J. Nanopart. Res.* **2014**, *16*, 2526. [CrossRef]

29.   Zafar, N.; Uzair, B.; Niazi, M.B.K.; Sajjad, S.; Samin, G.; Arshed, M.J.; Rafiq, S. Fabrication & characterization of chitosan coated biologically synthesized TiO₂ nanoparticles against PDR *E. coli* of veterinary origin. *Adv. Polym. Technol.* **2020**, *2020*, 8456024.

30.   Liu, P.; Dai, Y.-N.; Zhang, J.-P.; Wang, A.-Q.; Wei, Q. Chitosan-alginate nanoparticles as a novel drug delivery system for nifedipine. *Int. J. Biomed. Sci.* **2008**, *4*, 221.

31.   Jorgensen, J.H.; Turnidge, J.D. Susceptibility test methods: Dilution and disk diffusion methods. In *Manual of Clinical Microbiology*, 11th ed.; Jorgensen, J., Pfaller, M., Carroll, K., Funke, G., Landry, M., Richter, S., Warnock, D., Eds.; ASM Press: Washington, DC, USA, 2015; Chapter 71; pp. 1253–1273.

32.   EUCAST. European Committee on Antimicrobial Susceptibility Testing. Breakpoint Tables for Interpretation of MICs and Zone Diameters Version 6.0. 2016. Available online: www.eucast.org (accessed on 10 January 2017).

33. Uzair, B.; Ahmed, N.; Ahmad, V.U.; Mohammad, F.V.; Edwards, D.H. The isolation, puri¢cation and biological activity of a novel antibacterial compound produced by *Pseudomonas stutzeri*. *FEMS Microbiol. Lett.* **2008**, *279*, 243–250. [CrossRef]

34. Berney, M.; Hammes, F.; Bosshard, F.; Weilenmann, H.U.; Egli, T. Assessment and Interpretation of Bacterial Viability by Using the LIVE/DEAD BacLight Kit in Combination with Flow Cytometry. *Appl. Environ. Microbiol.* **2007**, *73*, 3283–3290. [CrossRef]

35. Khan, B.A.; Ullah, S.; Khan, M.K.; Alshahrani, S.M.; Braga, V.A. Formulation and evaluation of Ocimumbasilicum-based emulgel for wound healing using animal model. *Saudi Pharm. J.* **2020**, *28*, 1842–1850. [CrossRef]

36. Caputo, F.; Mameli, M.; Sienkiewicz, A.; Licoccia, S.; Stellacci, F.; Ghibelli, L.; Traversa, E. A novel synthetic approach of cerium oxide nanoparticles with improved biomedical activity. *Sci. Rep.* **2017**, *7*, 1–13. [CrossRef] [PubMed]

37. Dobrovolskaia, M.A.; Clogston, J.D.; Neun, B.W.; Hall, J.B.; Patri, A.K.; McNeil, S.E. Method for analysis of nanoparticle hemolytic properties in vitro. *Nano Lett.* **2008**, *8*, 2180–2187. [CrossRef] [PubMed]

38. Dudley, M.N.; Ambrose, P.G.; Bhavnani, S.M.; Craig, W.A.; Ferraro, M.J.; Jones, R.N.; Clinical, Antimicrobial Susceptibility Testing Subcommittee of the Clinical and Laboratory Standards Institute. Background and rationale for revised Clinical and Laboratory Standards Institute interpretive criteria (breakpoints) for Enterobacteriaceae and *Pseudomonas aeruginosa*: I. Cephalosporins and aztreonam. *Clin. Infect. Dis.* **2013**, *56*, 1301–1309. [PubMed]

39. CLSI. *M100-S26: Performances Standards for Antimicrobial Susceptibility Testing*; Twenty-Fourth Informational Supplement; Clinical Laboratory Standards Institute: Wayne, PA, USA, 2016.

40. Bokare, A.; Sanap, A.; Pai, M.; Sabharwal, S.; Athawale, A.A. Antibacterial activities of Nd doped and Ag coated TiO_2 nanoparticles under solar light irradiation. *Colloids Surf. B Biointerfaces* **2013**, *102*, 273–280. [CrossRef]

41. Senthilkumar, P.; Yaswant, G.; Kavitha, S.; Chandramohan, E.; Kowsalya, G.; Vijay, R.; Sudhagar, B.; Kumar, D.R.S. Preparation and characterization of hybrid chitosan-silver nanoparticles (Chi-Ag NPs); A potential antibacterial agent. *Int.J. Biol. Macromol.* **2019**, *141*, 290–298. [CrossRef]

42. Hussein, E.M.; Desoky, W.M.; Hanafy, M.F.; Guirguis, O.W. Effect of TiO_2 nanoparticles on the structural configurations and thermal, mechanical, and optical properties of chitosan/TiO_2 nanoparticle composites. *J. Phys. Chem. Solids* **2021**, *152*, 109983. [CrossRef]

43. Mohamed, N. Synthesis of Hybrid Chitosan Silver Nanoparticles Loaded with Doxorubicin with Promising Anti-cancer Activity. *Biol. Nano Sci.* **2020**, *10*, 758–765. [CrossRef]

44. Georgekutty, R.; Seery, M.K.; Pillai, S.C. A highly efficient Ag-ZnOphotocatalyst: Synthesis, properties, and mechanism. *J. Phys. Chem. C* **2008**, *112*, 13563–13570. [CrossRef]

45. Lee, J.H.; Jung, K.Y.; Park, S.B. Modification of titania particles by ultrasonic spray pyrolysis of colloid. *J. Mater. Sci.* **1999**, *34*, 4089–4093. [CrossRef]

46. Li, J.; Xie, B.; Xia, K.; Li, Y.; Han, J.; Zhao, C. Enhanced antibacterial activity of silver doped titanium dioxide-chitosan composites under visible light. *Materials* **2018**, *11*, 1403. [CrossRef] [PubMed]

47. Wiącek, A.E.; Gozdecka, A.; Jurak, M. Physicochemical characteristics of chitosan–TiO_2 biomaterial. 1. Stability and swelling properties. *Ind. Eng. Chem. Res.* **2018**, *57*, 1859–1870. [CrossRef]

48. Hoseinzadeh, E.; Makhdoumi, P.; Taha, P.; Hossini, H.; Stelling, J.; Amjad Kamal, M. A review on nano-antimicrobials: Metal nanoparticles, methods and mechanisms. *Curr. Drug Metab.* **2017**, *18*, 120–128. [CrossRef] [PubMed]

49. Wang, L.; Hu, C.; Shao, L. The antimicrobial activity of nanoparticles: Present situation and prospects for the future. *Int. J. Nanomed.* **2017**, *12*, 1227. [CrossRef] [PubMed]

50. Hanna, D.H.; Saad, G.R. Encapsulation of ciprofloxacin within modified xanthan gum- chitosan based hydrogel for drug delivery. *Bioorg. Chem.* **2019**, *84*, 115–124. [CrossRef] [PubMed]

51. Shahverdi, A.; Fakhimi, A.; Shahverdi, H.; Minaian, S. Synthesis and effect of silver nanoparticles on the anti-bacterial activity of different antibiotics against *Staphylococcus aureus* and *Escherichia coli*. *Nanomed. Nanotechnol. Biol. Med.* **2007**, *3*, 168–171. [CrossRef]

52. Ashmore, D.A.; Chaudhari, A.; Barlow, B.; Barlow, B.; Harper, T.; Vig, K.; Miller, M.; Singh, S.; Nelson, E.; Pillai, S. Evaluation of *E. coli* inhibition by plain and polymer-coated silver nanoparticles. *Rev. Inst. Med. Trop. São Paulo* **2018**, *60*, e18. [CrossRef] [PubMed]

53. Carter, E.A.; Frank, E.P.; Hunter, P.A. Cytometric evaluation of antifungal agents. In *Flow Cytometry in Microbiology*; Lloyd, D., Ed.; Springer: London, UK, 1993; pp. 111–120.

54. Vanhauteghem, D.; Audenaert, K.; Demeyere, K.; Hoogendoorn, F.; Janssens, G.P.; Meyer, E. Flow cytometry, a powerful novel tool to rapidly assess bacterial viability in metal working fluids: Proof-of-principle. *PLoS ONE* **2019**, *14*, e0211583. [CrossRef]

55. Cui, Z.; Zheng, Z.; Lin, L.; Si, J.; Wang, Q.; Peng, X.; Chen, W. Electrospinning and crosslinking of polyvinyl alcohol/chitosan composite nanofiber for transdermal drug delivery. *Adv. Polym. Technol.* **2018**, *37*, 1917–1928. [CrossRef]

56. Shahriar, S.; Mondal, J.; Hasan, M.N.; Revuri, V.; Lee, D.Y.; Lee, Y.-K. Electrospinningnanofibers for therapeutics delivery. *Nanomaterials* **2019**, *9*, 532. [CrossRef]

57. Shah, A.; Buabeid, M.A.; Arafa, E.-S.A.; Hussain, I.; Li, L.; Murtaza, G. The wound healing and antibacterial potential of triple-component nanocomposite (chitosan-silver-sericin) films loaded with moxifloxacin. *Int. J. Pharm.* **2019**, *564*, 22–38. [CrossRef]

58. Campos, D.A.M.; Diebold, Y.; Carvalho, E.L.; Sánchez, A.; Alonso, M.J. Chitosan nanoparticles as new ocular drug delivery systems: In vitro stability, in vivo fate, and cellular toxicity. *Pharm. Res.* **2004**, *21*, 803–810. [CrossRef]

59. Tomankova, K.; Horakova, J.; Harvanova, M.; Malina, L.; Soukupova, J.; Hradilova, S.; Kejlova, K.; Malohlava, J.; Licman, L.; Dvorakova, M.; et al. Cytotoxicity, cell uptake and microscopic analysis of titanium dioxide and silver nanoparticles in vitro. *Food Chem. Toxicol.* **2015**, *82*, 106–115. [CrossRef]

60. Li, S.-Q.; Zhu, R.-R.; Zhu, H.; Xue, M.; Sun, X.-Y.; Yao, S.-D.; Wang, S.-L. Nanotoxicity of TiO_2 nanoparticles to erythrocyte in vitro. *Food Chem. Toxicol.* **2008**, *46*, 3626–3631. [CrossRef] [PubMed]

61. Choi, J.; Reipa, V.; Hitchins, V.M.; Goering, P.L.; Malinauskas, R.A. Physicochemical characterization and invitro hemolysis evaluation of silver nanoparticles. *Toxicol. Sci.* **2011**, *123*, 133–143. [CrossRef] [PubMed]

62. Vijayalakshmi, K.; Sivaraj, D. Synergistic antibacterial activity of barium doped TiO_2 nanoclusters synthesized by microwave processing. *RSC Adv.* **2016**, *6*, 9663–9671. [CrossRef]

63. Rabea, E.I.; Badawy, M.E.-T.; Stevens, C.V.; Smagghe, G.; Steurbaut, W. Chitosan as antimicrobial agent: Applications and mode of action. *Biomacromolecules* **2003**, *4*, 1457–1465. [CrossRef] [PubMed]

64. Qian, T.; Su, H.; Tan, T. The bactericidal and mildew-proof activity of a TiO_2–chitosan composite. *J. Photochem. Photobiol. A Chem.* **2011**, *218*, 130–136. [CrossRef]

65. Campoli-Richards, D.M.; Monk, J.P.; Price, A.; Benfield, P.; Todd, P.A.; Ward, A. Ciprofloxacin. *Drugs* **1988**, *35*, 373–447. [CrossRef] [PubMed]